C.P. No. 249
(18,012)
A.R.C. Technical Report

C.P. No. 249
(18,012)
A.R.C. Technical Report

MINISTRY OF SUPPLY

AERONAUTICAL RESEARCH COUNCIL

CURRENT PAPERS

Measurements of Pitching Moment Derivatives for a Series of Rectangular Wings at Low Wind Speeds

By

P. R. Guyett, B.Sc. and D. E. G. Poulter, G.I.Mech.E.

LONDON: HER MAJESTY'S STATIONERY OFFICE

1956

SEVEN SHILLINGS NET

C.P. No. 249

U.D.C. No. 533.691.13 : 533.6.013.152 : 532.6.011.3

Report No. Structures 185

June, 1955

ROYAL AIRCRAFT ESTABLISHMENT

Measurements of pitching moment derivatives for a series of rectangular wings at low wind speeds

by

P. R. Guyett, B.Sc.

and

D. E. G. Poulter, G.I.Mech.E.

SUMMARY

The direct aerodynamic moments for pitching oscillations have been measured on a series of rectangular wings having aspect ratios between 2 and 8 for axis positions at the wing leading edges and trailing edges. Two of the wings were also tested with single end plates which were aerodynamically effective in doubling the wing geometric aspect ratio. The measurements were made at low speeds in an open jet wind tunnel and covered the range of frequency parameter (based on wing chord) 0.13 to 0.39. The results are in general agreement with theoretical results due to Lawrence and Gerber.

Similar tests were also made on a wing fitted with two end plates in an attempt to obtain results for two-dimensional flow. The results do not agree with other experimental results and two-dimensional theoretical values and indicate that wind tunnel interference is important for this test configuration.

LIST OF CONTENTS

		Page
1	Introduction	4
2	Method of reducing the wing inertia-force reactions at the force measuring points	4
3	Apparatus	5
	3.1 Wind tunnel	5
	3.2 Wing models	5
	3.3 Wing supports	5
	3.4 Excitation equipment	6
	3.5 Frequency measurement	6
	3.6 Force measurement	7
4	Method	7
5	Test programme	8
6	Presentation of results	8
	6.1 Non-dimensional derivative coefficients	8
	6.2 Moment coefficients	9
	6.3 Resultant moments and phase angles	9
7	Discussion of results and comparison with theory	10
	7.1 Accuracy of measurements	10
	7.2 Still-air damping	10
	7.3 Wings of finite aspect ratio	10
	7.31 Effectiveness of single end plates	10
	7.32 Theoretical results	11
	7.33 Comparison with theory	11
	7.4 Wing fitted with two end plates	12
8	Conclusions	13
Acknowledgments		14
References		14
Appendix I -	Calculation of the galvanometer response to the input signal	16

LIST OF TABLES

	Table
Results for pitching oscillations about the leading edge	I
Results for pitching oscillations about the trailing edge	II

LIST OF ILLUSTRATIONS

	Figure
Spring system for inertia balancing	1
Arrangement of rig in wind tunnel working section	2
Arrangement of end plates	3
Force measuring unit	4
The commutator and brush arrangement	5
Gauge output signal and switching	6
Velocity traverses on model spanwise centre line	7
Moment coefficients versus V and V^2	8
Variation of the stiffness moment derivative $(-m_\theta)$ with frequency parameter: pitching about leading edge	9
Variation of the stiffness moment derivative m_θ with frequency parameter: pitching about trailing edge	10
Variation of the stiffness moment derivative with $\frac{1}{\text{aspect ratio}}$ for wings pitching about their leading edges at $\nu = 0.15$	11
Variation of the stiffness moment derivative with $\frac{1}{\text{aspect ratio}}$ for wings pitching about their trailing edges at $\nu = 0.15$	12
Variation of resultant moment and phase angle with frequency parameter: pitching about leading edge	13
Variation of resultant moment and phase angle with frequency parameter: pitching about trailing edge	14
Variation of $(-m_\theta)$ with frequency parameter for wing pitching about its leading edge in two-dimensional flow	15
Variation of $(-\nu m_{\dot\theta})$ with frequency parameter for wing pitching about its leading edge in two-dimensional flow	16
Variation of m_θ with frequency parameter for wing pitching about its trailing edge in two-dimensional flow	17
Variation of $(-\nu m_{\dot\theta})$ with frequency parameter for wing pitching about its trailing edge in two-dimensional flow	18

1 Introduction

Values of the aerodynamic forces on oscillating aerofoil surfaces are required for the estimation of aircraft flutter speeds and in related problems. This information is needed for each practical aerofoil shape and its associated modes of oscillation.

Present knowledge of these forces is based largely on theoretical investigations, although experimental work has been done on the Continent, and in the U.S.A., as well as in this country. Experimental investigations can most easily be made for rigid modes of oscillation, that is, modes in which there is no elastic deformation of the aerofoil. The results are required for comparison with theoretical results to assess the accuracy of the theoretical method for simple modes before it is extended to deformation modes.

This report describes measurements of the direct aerodynamic moments for a series of unswept rigid rectangular wings of various aspect ratios oscillating in pitch about their leading or trailing edges, at low wind-speeds. The tests were made primarily on plain full-span wings, but tests were also made on two wings fitted with single end plates, and on one wing fitted with two end plates. These additional tests were to establish the effectiveness of the end plates, and to provide a means for obtaining results for twice the wing geometric aspect ratios and for nominally two-dimensional flow.

The aerodynamic moments were found by a direct measurement of the moment required to maintain the pitching oscillation of the wing in the airstream. Measurements were made in the range of frequency parameter (based on wing chord) between 0.13 and 0.39 at Reynolds numbers between 0.38×10^6 and 0.13×10^6 respectively.

The results for the wings of finite span have been compared with the theories of W. P. Jones[1] (1943) and Lawrence and Gerber[2] (1952). Both give results for rectangular wings oscillating in rigid modes in incompressible flow: Jones for aspect ratios of 4 and 6, and Lawrence and Gerber for aspect ratios of 2 and 4. The results for the wing oscillating in nominally two-dimensional flow have been compared with derivatives tabulated by Minhinnick[3] (1950).

All the experimental results are subject to wind tunnel corrections but so far as the writers know these corrections have not been determined for oscillating wings in a circular section open-jet wind tunnel of the type used in the present tests. There is, however, substantial agreement between the uncorrected results and theory except for the two-dimensional flow conditions. Tentative corrections have been applied to the stiffness derivatives based on the static wind tunnel corrections and are greatest for the two-dimensional flow tests and improve the agreement of the stiffness derivatives with theory. Experimental results for two-dimensional flow in a closed rectangular wind tunnel, including the appropriate oscillatory corrections, have been published by Bergh and Ijff[4] (1953) based on tests by Greidanus, van de Vooren and Bergh[5] (1952). These results are in general agreement with theory, which suggests that the wind tunnel corrections for the present tests simulating two-dimensional flow are important.

2 Method of reducing the wing inertia force reactions at the force measuring points

In techniques in which the aerodynamic forces on oscillating surfaces are measured directly account must be taken of the inertia force reactions at the measuring points. In a sinusoidal oscillation springs can be used to reduce or eliminate the unwanted inertia reactions at the measuring points.

This method was followed in the present tests, in which the moment about an axis of pitch only was measured, and is described in detail below.

The wing and associated spring arrangement is shown in Fig.1. The free end of the earthed linear spring of stiffness k is attached to the rod which oscillates in a direction perpendicular to the mean plane of the wing.

Let F_1, acting along the axis of the rod, be the only external force acting on the system which has a moment about the axis of pitch.

If the wing and rod behave as rigid bodies the following pitching moment equation of motion applies:-

$$F_1 \ell - k \ell^2 \theta = I\ddot{\theta} + D\dot{\theta} ,$$

where I is the pitching moment of inertia of the wing and rod, and D represents the total (still air) damping.

If the wing is made to oscillate at a frequency ω near its natural frequency $\ell \sqrt{k/I}$, then $\theta = \theta e^{i\omega t}$ and $\omega^2 I \approx k\ell^2$. Then

$$F_1 \ell = (k\ell^2 - \omega^2 I)\theta + i\omega D\theta \approx i\omega D\theta . \qquad (1)$$

The exciting force F_1 required thus consists mainly of a quadrature component balancing the damping. If the wing is then oscillated in the airstream at the same frequency ω, the additional in phase and quadrature components of the required force F_1 (which will be large compared with the still air forces) give directly the additional aerodynamic forces acting on the wing.

3 Apparatus

3.1 Wind tunnel

The tests were made in the RAE 5 ft diameter open jet wind tunnel.

3.2 Wing models

Each wing was of rectangular plan form, of 6" chord, and had a symmetrical 10% thickness to chord ratio. The wing section was to RAE 101 profile. Four wings were built having spans of 48", 30", 19.5" and 12", giving aspect ratios of 8, 5, 3.25 and 2 respectively. All the wings were of sandwich construction having a 16 SWG mild steel sheet at the section chord line flanked by solid spruce blocks shaped to the aerofoil contour. At the tips, on the line of the leading and trailing edges, and at intermediate positions on the leading and trailing edges, the steel sheet was extended to form attachment lugs for the wing supports. Lightening holes were cut out of the centre of the steel sheet and the rear of the sheet was cut away between the lugs and plywood inserted to form the trailing edge. The spruce, mild steel, and plywood were bonded together with 'Araldite'.

3.3 Wing supports

The wings were mounted vertically in the centre of the wind stream and allowed freedom to pitch about either their leading or trailing edges.

The required axis of pitch was defined by two steel pins, attached one at each wing tip to the appropriate lugs, which fitted into bearings made from steel washers. The washers were each held by four horizontal 24 SWG piano

wires, two going forward from the washer to attach to the structure of wind tunnel entry nozzle, and the remaining two going back to attach to the frame of the safety screen at the end of the working section. Vertical wires from the working section floor and roof were attached to the ends of the axis pins projecting through the washers. Additional bracing wires attaching to the intermediate lugs on the pitching axis were fitted across the tunnel (Fig.2).

For the tests in which wings were fitted with end plates an 18 SWG aluminium plate was attached directly to the wing tip and oscillated with the wing over the centre of a larger plywood plate which was fixed in position in the working section on four streamlined tubes extending from the floor to the roof structure above. Dimensions of the metal and plywood end plates are given in Fig.3. The gap between the two plates and the size of the cut-outs in the wooden plate, to allow the attachment lugs to pass through, were made as small as practicable. Velocity traverses with the wing removed were made between the two plywood end plates in position for the tests on the wing of nominally infinite aspect ratio and above a single plywood end plate in position for the tests on a wing of nominal aspect ratio 6.5. The velocity distributions are shown in Fig.7. They indicate that the flow was reasonably uniform at the wing position.

3.4 Excitation equipment

The wing oscillations were maintained by forcing with a swash plate exciter. The angle of tilt of the swash plate could be smoothly varied, and altered the amplitude of oscillation of a plunger rod projecting from the exciter body. Sinusoidal forcing from the plunger was transmitted through a spring and connecting rod to the mid-chord point on the wing centre line. A force-sensitive measuring unit (section 3.6) was built into the connecting rod and the spring for inertia balancing was attached to the rod on the wing side of this unit. Fig.2 shows the system and its supports.

Under test it was found that the reaction of the inertia balancing spring forced a vibration in the support pillar. To overcome this an arm, pivoted in the pillar, and linked to the exciter end of the member connected to the wing was mass loaded in such a way that the force reaction on its pivot balanced the spring reaction and reduced the pillar vibration to an acceptable value.

3.5 Frequency measurement

The test method of reducing the inertia force reactions (see section 2) depends, for correct measurement of the superimposed loads, upon maintaining a constant frequency of oscillation.

To provide an accurate means of measuring the frequency an electronic counter was developed which enabled the time for a number of wing oscillations to be found correct to $\frac{1}{600}$th of a second. A similar counter having a wider application is described by Hicks[6].

At a frequency of 5 cps the mean time for 20 oscillations could therefore be determined to an accuracy of 1 part in 2400. The counter was made to operate automatically at approximately 10 second intervals.

Manual adjustment was made to the field resistance of the shunt wound D.C. motor driving the exciter to maintain the mean frequency generally to within 2 or 3 parts in 2400 of the chosen frequency.

3.6 Force measurement

The force required to maintain the wing pitching oscillations was measured at a unit in the rod connected to the wing. The measuring unit was developed to provide a large signal output and yet have the high stiffness to applied load generally required in force measurements on oscillating bodies.

Fig.4 shows the unit. The tensioned diagonal strips each carry a wire resistance strain gauge forming one arm of a Wheatstone bridge. An axial load between the centre connection and the body of the unit results in an increase in tension in one pair of strips and a decrease in tension in the other pair of strips producing a current, proportional to the load, in the galvanometer arm of the bridge circuit.

Output from the Wheatstone bridge was supplied to one of two pairs of brushes bearing at 180° on the segments of a two segment commutator mounted on the exciter shaft and rotating at the oscillation frequency. Fig.5 shows the commutator and the arrangement of the brushes. The two insulated centre segments each had an outer slip ring which was directly connected to the galvanometer. The gauge output was thus reversed in direction by the commutator at half-cycle intervals to produce a signal having a mean D.C. level measured by the galvanometer. The gauge output could also be switched to the second pair of brushes at 90° to the first. Calculations of the galvanometer response are given in Appendix I. In a sinusoidal oscillation in which the forces depend linearly upon velocity and displacement the galvanometer readings allow the amplitude of the gauge output and its phase relation to the commutator to be found. The commutator rotation was not, however, at a fixed phase relation to the wing motion since the wing forcing was applied through the filtering spring. A strain gauged cantilever strip was therefore attached to the connecting member to the wing and wired so that its output could also be supplied to the brushes on the commutator and measured by the galvanometer. The output from these gauges was in-phase with the wing motion and thus from the two sets of measurements the components of the force unit output signal in-phase and in quadrature with the wing motion was found.

4 Method

The effect of frequency parameter upon the aerodynamic derivatives for the wings oscillating at a set circular frequency was found by making measurements over a range of wind speeds. The frequency of oscillation chosen was 4.97 cps.

For each test condition, the stiffness of the inertia balancing spring was adjusted until the difference between the inertia force, in still air, and the spring reaction, as measured at the force unit at the chosen amplitude and frequency of oscillation, was small compared with the anticipated aerodynamic load. This small in-phase force and the accompanying in quadrature damping force required to overcome the still air aerodynamic and apparatus damping were then measured. Measurements of the force needed to maintain the oscillation at the same frequency and amplitude were made at wind speeds of 40, 60, 80, 100 and 120 ft/sec. After the wind-on tests a further set of measurements were made in still air. The aerodynamic forces due to the wind stream at each speed were taken to be the difference between the wind-on measurements and the measurements made in still air.

The in-phase forces found in this way correspond to the aerodynamic forces due to displacement alone, since the virtual inertia force, which is present both with the wind-on and in still air, is excluded by the subtraction. Similarly, the derived forces in quadrature with the wing motion do not include the still air damping.

The force unit was calibrated dynamically by attaching masses to the wing and measuring the extra output in an oscillation at the test frequency and

amplitude. These extra forces were in-phase with the wing motion and provided a check on the phasing at the commutator. Calibration loads covering the range of the aerodynamic loads were applied immediately before or after each set of wind-on tests.

5 Test programme

Results were obtained for the following wing conditions:-

Aspect Ratio	Wing condition	Pitching Axis
2	Full span	L.E. & T.E.
3.25	Full span	L.E. & T.E.
4 *	Wing of geometric aspect ratio 2 with single end plate	L.E.
5	Full span	L.E. & T.E.
6.5*	Wing of geometric aspect ratio 3.25 with single end plate	L.E.
8	Full span	L.E.
∞ *	Wing of geometric aspect ratio 3.25 with two end plates	L.E. & T.E.

* Nominal.

6 Presentation of results

6.1 Non-dimensional derivative coefficients

The aerodynamic stiffness and damping moments about the axis of pitch may be expressed in terms of the non-dimensional equivalent constant strip derivatives, m_θ and $m_{\dot{\theta}}$, in the following way:-

$$M_\theta' = m_\theta \rho V^2 S c \theta_o , \qquad (2)$$

$$M_\theta'' = m_{\dot{\theta}} \nu \rho V^2 S c \theta_o , \qquad (3)$$

where M_θ' = amplitude of the stiffness component of the resultant aerodynamic moment (in-phase with the motion) and

M_θ'' = amplitude of the damping component of the resultant aerodynamic moment (in quadrature with the motion) (+ve moment forcing wing nose up)

ρ = air density

V = wind speed

S = wing area

c = wing chord

θ_o = pitching amplitude (angle of pitch measured +ve wing nose up)

ν = frequency parameter $\frac{\omega c}{V}$

ω = circular frequency of oscillation.

The above derivatives m_θ and $m_{\dot\theta}$ are expressed in terms of the non-dimensional equivalent constant strip derivatives referred to the leading edge (see Templeton[7], 1953) as follows

Pitching about the leading edge,

$$m_\theta = m_\alpha ,$$

$$m_{\dot\theta} = m_{\dot\alpha} ,$$

pitching about the trailing edge,

$$m_\theta = \ell_\alpha + m_\alpha - \ell_z - m_z ,$$

$$m_{\dot\theta} = \ell_{\dot\alpha} + m_{\dot\alpha} - \ell_{\dot z} - m_{\dot z} .$$

The measured values of $m_{\dot\theta}$ and $\nu m_{\dot\theta}$ are given fully in Tables I and II. The measured derivative m_θ for each of the wing conditions tested is plotted against frequency parameter in Figs. 9 and 10. The damping derivative $m_{\dot\theta}$ is not plotted for the reason given in section 7.1.

6.2 Moment coefficients

The equations at (2) and (3) may be rearranged and written,

$$\frac{M_\theta'}{\rho S c \theta_o} = m_\theta V^2 ,$$

$$\frac{M_\theta''}{\rho S c \theta_o} = m_{\dot\theta} V \omega c .$$

Fig.8 shows two typical examples of the moment coefficients $\frac{M_\theta'}{\rho S c \theta_o}$ and $\frac{M_\theta''}{\rho S c \theta_o}$ plotted against V^2 and V respectively.

Departure of the test points (each of which corresponds to a different frequency parameter) from a straight line through the origin indicates the variation of the derivative coefficients m_θ and $m_{\dot\theta}$ with frequency parameter.

6.3 Resultant moments and phase angles

The aerodynamic moments may also be expressed in terms of the non-dimensional resultant moment $\bar m$, and the phase angle, ε, by which it leads the motion vector, thus:-

$$\bar m = \sqrt{m_\theta^2 + \nu^2 m_{\dot\theta}^2} ,$$

$$\varepsilon = \tan^{-1} \frac{\nu m_{\dot\theta}}{m_\theta} .$$

The measured values of $\bar{m}$ and ε are given in Tables I and II, and are plotted against frequency parameter for each of the wings tested in Figs. 13 and 14.

7 Discussion of results and comparison with theory

7.1 Accuracy of measurements

The percentage accuracy of the experimental measurements depended upon the magnitude of the aerodynamic moments. At the lowest test wind speed, corresponding to a frequency parameter of 0.39, the magnitude of the resultant moment $\bar{m}$ could generally be measured to an accuracy of 5% and the phase angle ε to within 5°. At the higher wind speeds, corresponding to the lowest test frequency parameters, $\bar{m}$ could generally be measured to within 2% and ε to 2°.

Since the measured phase angles were small, it follows that the stiffness derivative m_{θ} was usually determined to a greater percentage accuracy than the damping derivative $m_{\dot{\theta}}$. It was therefore preferred to present the damping moments indirectly, in the form of resultant moment and phase angle, rather than directly, in the form of the derivative $m_{\dot{\theta}}$, as the direct presentation could give a misleading indication of the order of agreement between theory and experiment in relation to the accuracy of measurement.

7.2 Still-air damping

It has been pointed out in section 4 that the in quadrature moments found from the wind tunnel tests do not include the still air damping moments and consequently do not represent the total aerodynamic damping moment acting on the wing. The still air damping may be found from a separate measurement of the rate of decay of the pitching oscillation in still air.

For this experiment the wing of aspect ratio 2 was chosen and supported on knife edges to allow it to swing as a compound pendulum about its trailing edge. From measurements of the time of decay between two amplitudes and from similar measurements on a concentrated mass system, to determine the damping in the knife edges, the aerodynamic damping was found at a frequency of swing of 1.3 cps. The damping moment was expressed as $B\dot{\theta}$ and it was found that the coefficient B was approximately linearly proportional to the mean amplitude of swing. Bratt and Wight[8] (1945) have shown that B is also linearly proportional to the frequency of oscillation. Using these relationships the still air damping appropriate to the wind tunnel test amplitude and circular frequency represents a correction to the measured out-of-phase derivative of approximately $2\frac{1}{2}\%$ at $\nu = 0.13$ and 6% at $\nu = 0.39$. If the result is also applied to the wing of aspect ratio 2 pitching about its leading edge the corresponding correction is 1% at $\nu = 0.13$ and $3\frac{1}{2}\%$ at $\nu = 0.39$.

Since these corrections are fairly small and refer only to the test amplitudes and frequencies they have been omitted and no further tests on other wings were made.

7.3 Wings of finite aspect ratio

7.31 Effectiveness of single end plates

The effectiveness of the end plates can be judged by comparing the results for the wings fitted with single end plates with the results for the full span wings.

Fig. 13(a) - (f) shows the variation of the non-dimensional resultant moment $\bar{m}$ and the phase angle ε with frequency parameter for the wings

pitching about their leading edges. Fig. 9(a) - (f) shows the variation of the corresponding component derivative m_θ with frequency parameter. The results for aspect ratios of 2, 3.25, 5 and 8 are from tests on full span wings and the results for aspect ratios of 4 and 6.5 are from tests on wings of geometric aspect ratios of 2 and 3.25 fitted with single end plates.

The curves indicate, by convenient comparison with the plotted theoretical values, that the trends and magnitudes of the results for the wings with end plates are consistent with those for the full span wings. The discrepancies that exist are of the order of the experimental accuracy and of the differences between the results for the full span wings.

Further indication that the magnitudes of the results are consistent may be obtained by cross-plotting against aspect ratio or, more conveniently, its reciprocal. Aspect ratio has a much greater effect upon the magnitude of the stiffness derivative m_θ than upon the damping derivative $m_{\dot\theta}$, and m_θ is shown plotted, for a frequency parameter of 0.15, against the reciprocal of the aspect ratio in Fig.11.

The results thus show that to within the accuracy of the measurements and for the test oscillation the single end plates are effective in reflecting the flow conditions.

7.32 Theoretical results

The theoretical curves plotted in Figs. 9, 10, 13, 14 are based on the results due to Lawrence and Gerber for wings of aspect ratios 2 and 4 given in Ref.2 and the two-dimensional derivatives for Mach number 0 tabulated in Ref.3. The virtual inertia terms have been removed from the in-phase derivatives of Ref.2 to give the required stiffness derivatives. The stiffness and damping derivatives were then plotted against the reciprocal of the aspect ratio to give curves for each frequency parameter similar to those in Figs. 11 and 12. Derivatives were found from these curves for each of the test aspect ratios. Reference 2 does not, however, give results for damping derivatives at frequency parameters below 0.25. To facilitate comparison with the experimental results the theoretical curves have therefore been extended to join up smoothly with the appropriate values at zero frequency parameter.

The same theoretical data are given in Figs. 11 and 12, which also include theoretical values from W. P. Jones[1] for wings of aspect ratios 4 and 6.

7.33 Comparison with theory

At aspect ratios up to approximately 4 the theoretical stiffness moment derivative m_θ shows little variation with frequency parameter; above 4 the derivative begins to approach the two-dimensional condition in which there is a large variation over the test range of frequency parameter. The experimental results for the wings pitching about their leading edges also show for the lower aspect ratios that the derivative is practically independent of frequency parameter, but for the higher aspect ratios show an opposite-to-theoretical trend. For the wings pitching about their trailing edges, the experimental trend is slightly more pronounced than the theoretical trend. The variation of the measured derivatives with frequency parameter is, however, generally small and can best be seen by examining the moment coefficients, M_θ', which are directly proportional to the measured moments (see section 6.2). Two typical examples are shown in Fig.8. The amount by which each test point lies off the straight line through the origin is a measure of the variation of the derivative with frequency parameter.

The theoretical and experimental derivatives m_θ have also been cross plotted at frequency parameter 0.15 against the reciprocal of the aspect ratio

in Figs. 11 and 12. The graphs show results from the theories of Lawrence and Gerber[2] and Jones[1] and indicate that a small difference exists between them for pitching motion about the leading edge but that they agree closely for pitching motion about the trailing edge. The experimental results for pitching about the leading edge are in closer agreement with the Lawrence and Gerber results but are slightly greater for the low aspect ratios and are slightly smaller at the high aspect ratios. The experimental results for pitching motion about the trailing edge are in fairly close agreement with the theory.

The experimental results, however, are subject to wind tunnel corrections due to the finite extent of the jet stream. So far as the writers know these corrections have not been found for oscillating wings in an open jet circular section wind tunnel. From existing work in this subject (e.g. W.P. Jones[9], 1943) it appears that the corrections are greatest at low frequency parameter. At zero frequency parameter, which corresponds to the static condition, the corrections have been determined for the test wind tunnel, and, to establish the order of the correction, these static corrections have been applied to the stiffness moment derivatives* for frequency parameter 0.15. The resulting derivatives are included in Figs. 11 and 12. The magnitude of the correction is greatest for the wings of high aspect ratio and generally improves the agreement with theory for the wings pitching about their leading edges and makes it slightly worse for the wings pitching about their trailing edges.

The resultant moment $\bar{m}$ and the phase angle ε are shown plotted against frequency parameter in Figs. 13(a) - (f) and 14(a) - (c). The plotted experimental results are uncorrected for wind tunnel interference. The experimental resultant moment shows a general agreement with theory similar to that for the corresponding stiffness moment derivative m_θ, which forms its principal component. The measured phase angles for pitching motion about the leading edge are in close agreement with theory at the lowest test frequency parameters but at higher frequency parameters the measured phase angles are smaller than the theoretical phase angles by an amount generally greater than the experimental error. In pitching motion about the trailing edge the phase angles are in reasonable agreement.

7.4 Wing fitted with two end plates

The test results are given in Figs. 9(g) and 10(d) which show the variation of m_θ with frequency parameter and in Figs. 13(g) and 14(d) which show the variation of $\bar{m}$ and ε with frequency parameter. Values for the derivatives m_θ and $\nu m_{\dot{\theta}}$ are plotted against frequency parameter in Figs. 15 - 18.

Figs. 15-18 show that although the measured stiffness moment derivatives are of the same order of magnitude as the theoretical derivatives, the measured damping moment derivatives do not show the large theoretical variation with frequency parameter and are of considerably different magnitude, especially at low frequency parameter.

Included in the figures are corresponding experimental derivatives calculated from coefficients given by Bergh and Ijff in Ref.4. These coefficients are based on the results of tests made by Greidanus, van de Vooren, and Bergh[5] at the N.L.L. Amsterdam on a wing spanning a closed rectangular section wind tunnel. Wind tunnel corrections have been applied to the coefficients. The final derivatives are in fairly close agreement with theory and thus indicate that wind tunnel corrections are important for the arrangement used in the R.A.E. tests.

---

* The static corrections do not, of course, give any indication of the correction that should be applied to the damping derivatives.

The wind tunnel corrections depend upon the size and position of the end plates as well as upon the wind tunnel configuration. (Fig.3 shows the end plates in the working section.) For the end plates to have been fully effective in the tunnel they should have extended to the boundary of the jet stream in the direction perpendicular to the plane of the wing, forward to the entry nozzle, and behind the wing over the region in which the influence of the wake is important. Even under these conditions, however, the oscillatory corrections, so far as the writers know, have not been determined but the static corrections are given by Durand[10]. These corrections, strictly only appropriate at zero frequency parameter, have been applied to the stiffness moment derivatives and the results are plotted in Figs. 15 and 17. The amount of correction for the wing with end plates is twice as great as that for any of the other wing conditions (see Figs. 11 and 12) and considerably improves the agreement with theory. This correction again does not give any indication of the effect of the wind stream boundaries on the damping derivatives, for which there is the largest discrepancy between the measured results, but suggests that this may be important.

The amount of extension of the end plates behind the wing may also influence the measured moments. The plates extended one and one half chord lengths distance behind the trailing edge and within this length could reflect the free vortices from the wing. Beyond the edge of the plate the vortex system must clearly degenerate into a trail of finite width. The test configuration is thus equivalent to a wing of infinite span with its vortex trail cut off at a small distance behind the wing over all the wing span except for a section equal in width to the distance between the end plates. This effective loss of wake will influence the forces acting on the test section. Jordan[11] (1953) has found the effect on the derivatives for a wing of infinite span due to cutting off the whole of the vortex trail at a finite distance behind the wing. Results for various positions of the cut-off are given in Figs. 15-18. It may be seen that the effect on the stiffness moment derivatives is fairly small, but that for a cut-off at two chord lengths behind the wing (which is a close approximation to the test condition) the modified damping derivatives for pitching about the leading edge bear the same relation to the unmodified theoretical derivatives as the R.A.E. test results bear to the N.L.L. results, and for pitching about the trailing edge the modified damping derivatives are in agreement with the R.A.E. results. The R.A.E. test configuration differs, however, from that represented by Jordan due to the presence of the extended vortex trail of finite width. The likely effect of this vortex trail is to reduce the effective wing aspect ratio. The small variation of the measured derivatives with frequency parameter for instance is consistent with the results for wings of lower aspect ratio. Fig.16 also indicates that the effect of the possible cut-off of the extended vortex trail at the tunnel fan, distance nineteen chord lengths behind the wing, is negligible.

This examination of the flow conditions shows that there is evidence that the results for the wing fitted with two end plates, although not in agreement with the two-dimensional theoretical and other measured results, are not unexpected for the test configuration.

The agreement of the results for the wings fitted with single end plates with the results for the full span wings implies that the effect of cutting off the reflected vortex trail at the edge of the end plate under those test conditions is not so important.

8 Conclusions

(1) Values of the direct aerodynamic moments for rectangular wings oscillating in pitch about their leading and trailing edges, based on the calculated values of Lawrence and Gerber, are in fairly good agreement with the measured moments for both axes of pitch. The measured and calculated phase angles between the moment and displacement vectors for pitching oscillations about the

leading edge are in good agreement at the lowest test frequency parameters, but at higher frequency parameters the calculated phase angles are slightly greater than the measured angles. The corresponding phase angles for pitching oscillations about the trailing edge are in satisfactory agreement.

(2) Within the test range of measurements the single end plates fitted to rectangular wings oscillating about their leading edges are effective as aerodynamic reflector plates.

(3) Wind tunnel corrections are important for the test configuration simulating two-dimensional flow in which a rectangular wing was oscillated between two end plates mounted in the windstream of an open jet wind tunnel.

Acknowledgments

The authors wish to thank Mr. F. Smith, Mr. W. G. Molyneux, and Mr. D. R. Gaukroger for advice and assistance given during the tests.

REFERENCES

No.	Author	Title, etc.
1	W.P. Jones	Theoretical air-load and derivative coefficients for rectangular wings. R & M 2142. February 1943.
2	H.R. Lawrence E.H. Gerber	The aerodynamic forces on low aspect ratio wings oscillating in an incompressible flow. Journal of the Aeronautical Sciences, Vol.19, No.11. November 1952.
3	I.T. Minhinnick	Subsonic aerodynamic flutter derivatives for wings and control surfaces (compressible and incompressible flow). RAE Report No. Structures 87. July 1950. ARC 14,228, 14,885. 0.956.
4	H. Bergh J. Ijff	Application of experimental aerodynamic coefficients to flutter calculations. Report F.122 of the Nationaal Luchtvaartlaboratorium, Amsterdam. 1953.
5	J.H. Greidanus A.I. van de Vooren H. Bergh	Experimental determination of the aerodynamic coefficients of an oscillating wing in incompressible flow. Parts I - IV. Reports F.101-104 of the Nationaal Luchtvaartlaboratorium, Amsterdam. 1952.
6	W.D.T. Hicks	An electronic instrument for the accurate measurement of the frequency of structural oscillations. RAE Tech Note Structures 150. January 1955.
7	H. Templeton	The technique of flutter calculations. Current Paper No. 172.
8	J.B. Bratt K.C. Wight	The effect of mean incidence, amplitude of oscillation, profile and aspect ratio on pitching moment derivatives. R & M 2064. June 1945.

REFERENCES (Contd)

No.	Author	Title, etc.
9	W.P. Jones	Wind tunnel interference effect on the values of experimentally determined derivative coefficients for oscillating aerofoils. R & M 1912. August 1943.
10	W.F. Durand (Editor)	Aerodynamic Theory. Volume III, p.302. Reprinted edition. California Institute of Technology. January 1943.
11	P.F. Jordan	The harmonically oscillating wing with finite vortex trail. RAE Report No. Structures 148. July 1953. ARC 16,228. 0.1077. FM 1962.

APPENDIX I

Calculation of the Galvanometer Response to the Input Signal

The sine wave output from the gauge, $S_o \sin \omega t$, and the brush positions are shown in Fig.6(a). If this output is supplied to brushes 'A' then the signal to the galvanometer is the gauge output reversed in direction at angles ϕ, $\phi + 180^\circ$, $\phi + 360^\circ$, etc., and has the form shown in Fig.6(b).

The mean galvanometer reading

$$= - \int_{\phi}^{\phi+180^\circ} \frac{S_o \sin \omega t}{\pi} \, d(\omega t) = - \frac{2S_o}{\pi} \cdot \cos \phi .$$

If the gauge output is supplied to brushes 'B' then the switching occurs at angles $\phi + 90^\circ$, $\phi + 270^\circ$, etc., and the signal to the galvanometer has the form shown in Fig.6(c).

The mean galvanometer reading

$$= - \int_{\phi+90^\circ}^{\phi+270^\circ} \frac{S_o \sin \omega t}{\pi} \cdot d(\omega t) = \frac{2S_o}{\pi} \cdot \sin \phi .$$

TABLES OF RESULTS

All the results are uncorrected for wind tunnel interference. All results refer to oscillations about a mean incidence of 0°.

TABLE I

Results for pitching oscillations about the leading edge

Wing span 12". Aspect ratio 2. $\theta_0 = 5.08^{\circ}$.

ν	$(-m_{\theta})$	$(-\nu m_{\dot{\theta}})$	$\bar{m}$	$\varepsilon^{\circ} - 180^{\circ}$
0.131	0.280	0.080	0.291	15.8
0.158	0.289	0.098	0.305	18.7
0.197	0.308	0.119	0.330	21.2
0.262	0.310	0.141	0.341	24.5
0.393	0.282	0.213	0.353	37.1

Wing span 19.5". Aspect ratio 3.25. $\theta_0 = 5.04^{\circ}$.

ν	$(-m_{\theta})$	$(-\nu m_{\dot{\theta}})$	$\bar{m}$	$\varepsilon^{\circ} - 180^{\circ}$
0.131	0.390	0.085	0.400	12.4
0.158	0.394	0.103	0.407	14.7
0.197	0.388	0.127	0.408	18.1
0.262	0.391	0.166	0.425	23.0
0.393	0.448	0.260	0.519	30.1

TABLE I (Contd)

Wing span 12" with single end plate.
Nominal aspect ratio 4. $\theta_o = 5.14^o$.

ν	$(-m_\theta)$	$(-\nu m_\theta^*)$	$\bar{m}$	$\varepsilon^o - 180^o$
0.130	0.406	0.085	0.415	11.8
0.156	0.401	0.102	0.413	14.3
0.195	0.397	0.117	0.414	16.4
0.260	0.407	0.148	0.433	20.0
0.390	0.437	0.224	0.491	27.2

Wing span 30". Aspect ratio 5. $\theta_o = 5.13^o$.

ν	$(-m_\theta)$	$(-\nu m_\theta^*)$	$\bar{m}$	$\varepsilon^o - 180^o$
0.131	0.430	0.083	0.438	11.0
0.158	0.441	0.076	0.448	9.8
0.197	0.447	0.090	0.456	11.4
0.262	0.459	0.103	0.470	12.6
0.393	0.438	0.158	0.466	19.9

Wing span 19.5" with single end plate.
Nominal aspect ratio 6.5. $\theta_o = 5.09^o$.

ν	$(-m_\theta)$	$(-\nu m_\theta^*)$	$\bar{m}$	$\varepsilon^o - 180^o$
0.130	0.473	0.084	0.480	10.1
0.156	0.478	0.107	0.489	12.7
0.195	0.491	0.134	0.509	15.3
0.260	0.501	0.185	0.534	20.3
0.390	0.520	0.206	0.559	21.7

TABLE I (Contd)

Wing span 48". Aspect ratio 8. $\theta_o = 4.83^\circ$.

ν	$(-m_\theta)$	$(-\nu m^*_\theta)$	$\bar{m}$	$\varepsilon^\circ - 180^\circ$
0.131	0.496	0.066	0.501	7.6
0.158	0.493	0.088	0.501	10.1
0.197	0.498	0.099	0.508	11.3
0.262	0.539	0.114	0.551	12.0
0.393	0.548	0.162	0.571	16.5

Wing span 19.5" with two end plates.

Nominal aspect ratio ∞. $\theta_o = 4.94^\circ$.

ν	$(-m_\theta)$	$(-\nu m^*_\theta)$	$\bar{m}$	$\varepsilon^\circ - 180^\circ$
0.130	0.560	0.087	0.566	8.8
0.156	0.568	0.096	0.576	9.6
0.195	0.566	0.129	0.581	12.9
0.260	0.569	0.140	0.586	13.8
0.390	0.545	0.210	0.584	21.1

TABLE II

Results for pitching oscillations about the trailing edge

Wing span 12". Aspect ratio 2. $\theta_o = 5.08^\circ$.

ν	m_θ	$(-\nu m'_\theta)$	$\bar{m}$	$360^\circ - \varepsilon^\circ$
0.131	1.042	0.034	1.042	1.9
0.158	1.030	0.025	1.031	1.4
0.197	1.018	0.042	1.019	2.4
0.262	1.000	0.072	1.002	4.1
0.393	1.004	0.123	1.011	7.0

Wing span 19.5" Aspect ratio 3.25. $\theta_o = 4.84^\circ$.

ν	m_θ	$(-\nu m'_\theta)$	$\bar{m}$	$360^\circ - \varepsilon^\circ$
0.131	1.282	0.071	1.284	3.2
0.158	1.267	0.121	1.272	5.5
0.197	1.250	0.145	1.259	6.6
0.262	1.193	0.151	1.202	7.2
0.393	1.198	0.245	1.223	11.5

Wing span 30". Aspect ratio 5. $\theta_o = 4.98^\circ$.

ν	m_θ	$(-\nu m'_\theta)$	$\bar{m}$	$360^\circ - \varepsilon^\circ$
0.131	1.576	0.132	1.582	4.8
0.158	1.541	0.144	1.548	5.3
0.197	1.501	0.179	1.511	6.8
0.262	1.481	0.235	1.500	9.0
0.393	1.449	0.385	1.499	14.9

TABLE II (Contd)

Wing span 19.5" with two end plates.

Nominal aspect ratio ∞. $\theta_o = 5.13^\circ$.

ν	m_θ	$(-\nu m_{\dot{\theta}})$	$\bar{m}$	$360^\circ - \varepsilon^\circ$
0.130	1.699	0.173	1.708	5.8
0.156	1.633	0.183	1.643	6.4
0.195	1.622	0.229	1.639	8.0
0.260	1.556	0.284	1.582	10.3
0.390	1.502	0.438	1.564	16.3

Wt.2078 - CP249 - K3. Printed in Great Britain.

FIG 1

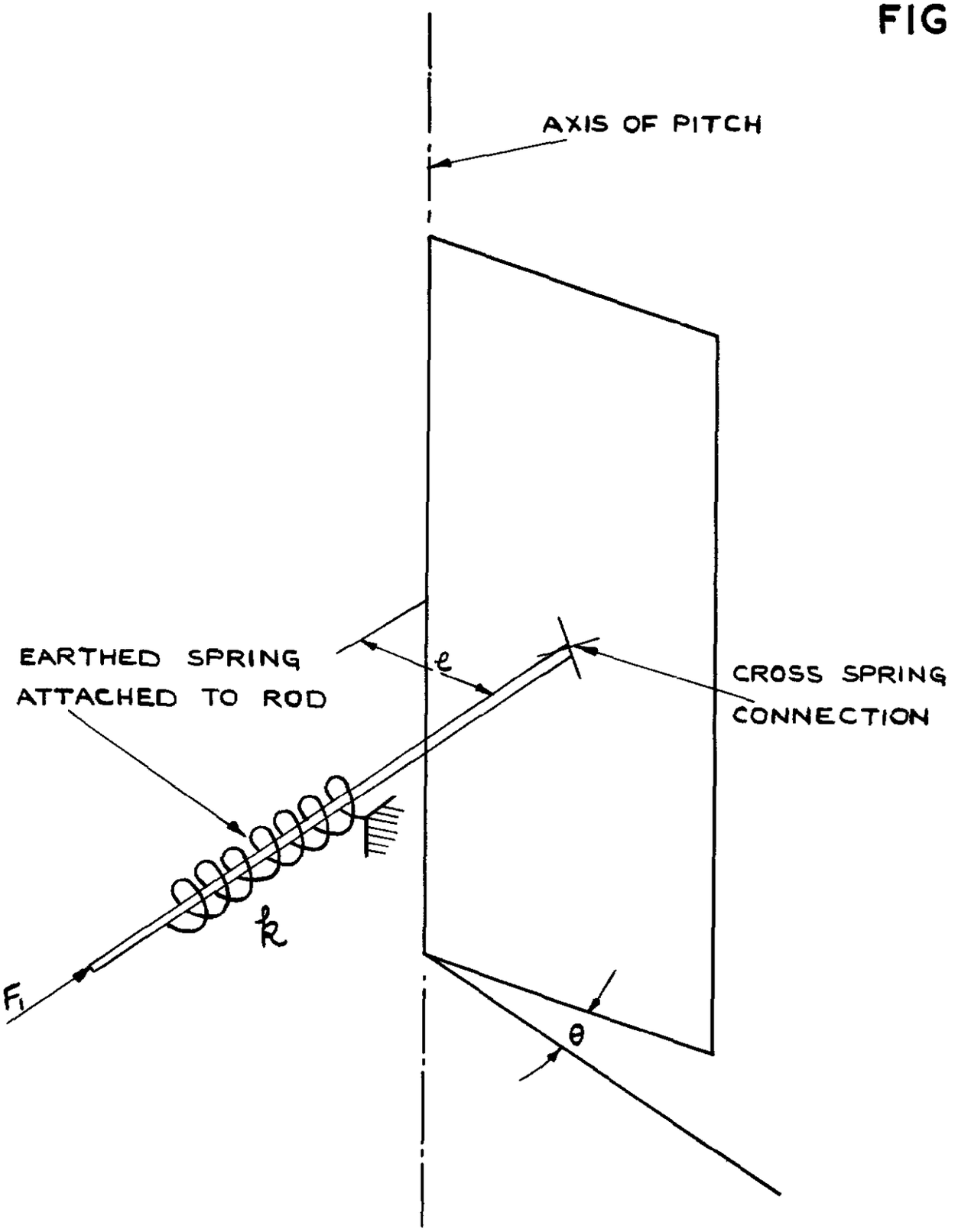

FIG 1. SPRING SYSTEM FOR INERTIA BALANCING.

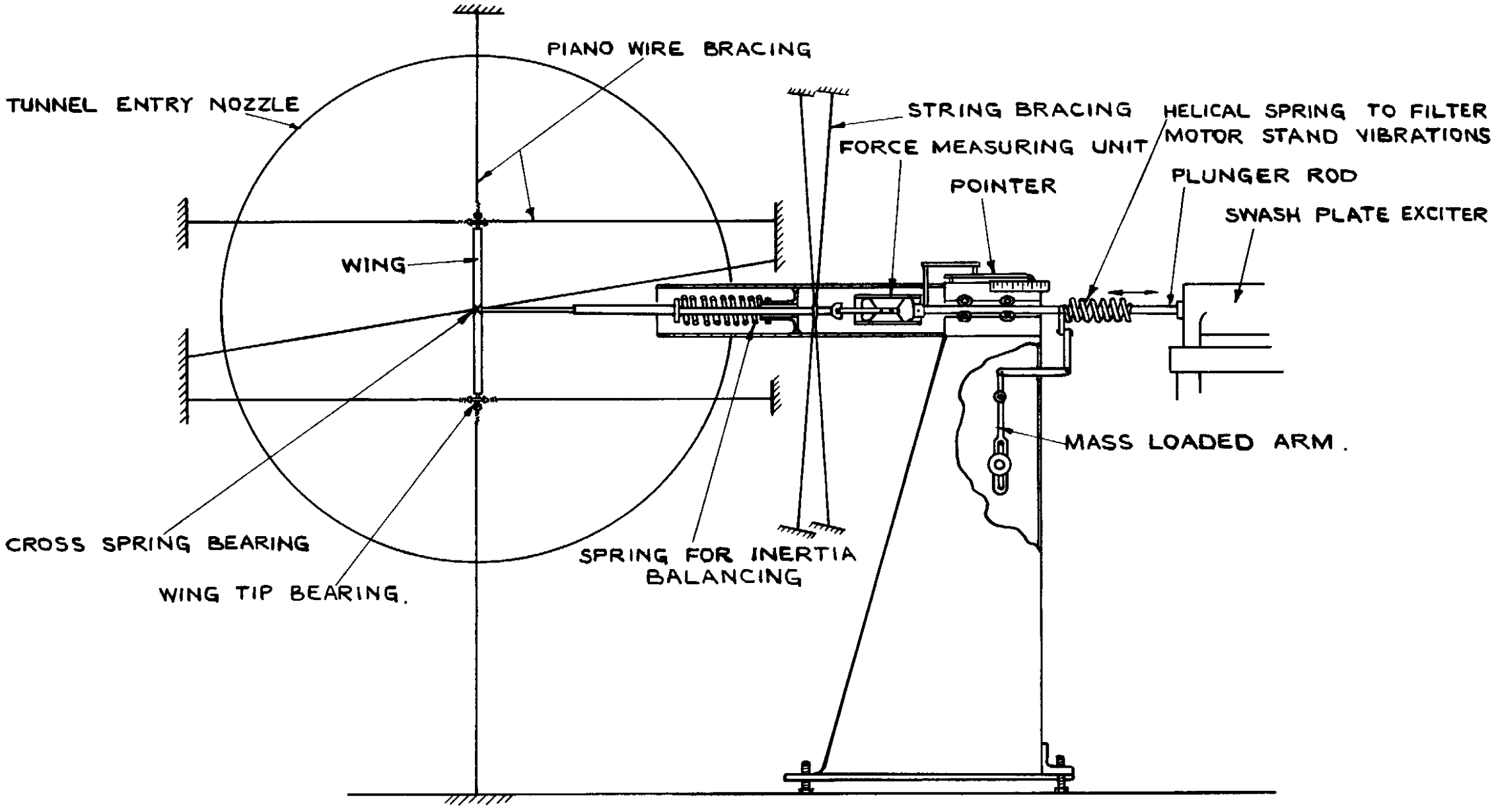

FIG. 2

FIG 2. ARRANGEMENT OF RIG IN WIND TUNNEL WORKING SECTION.

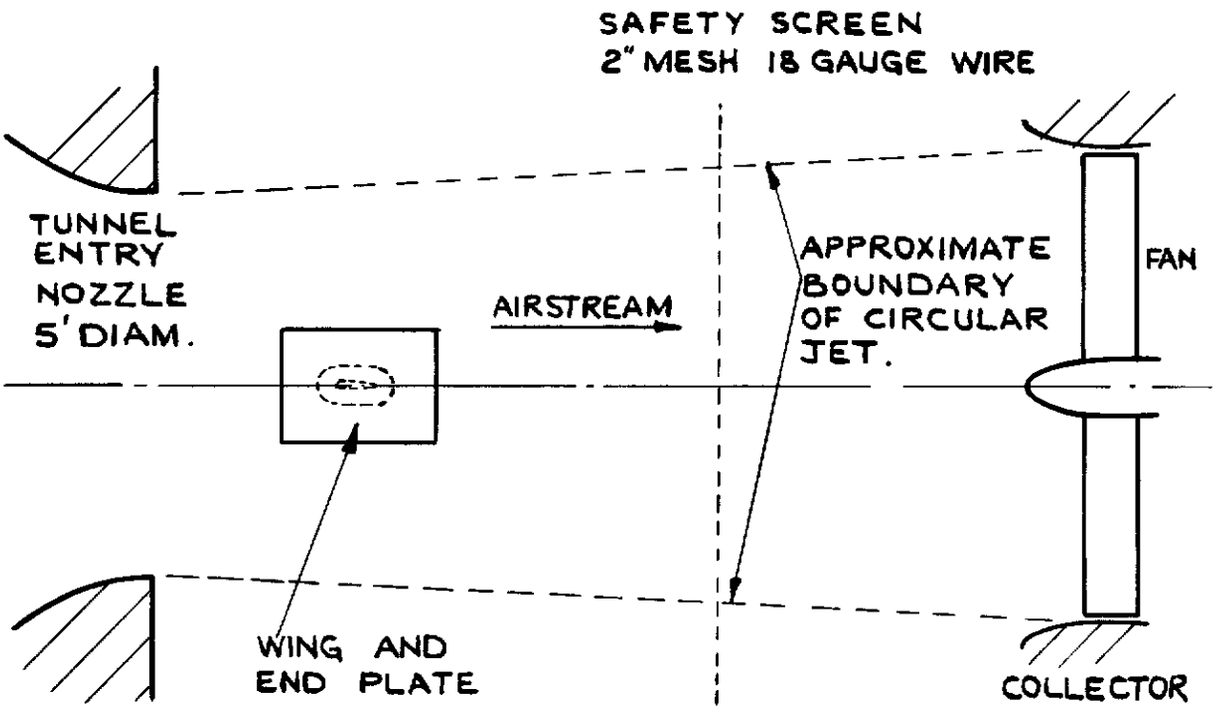

PLAN OF WORKING SECTION.

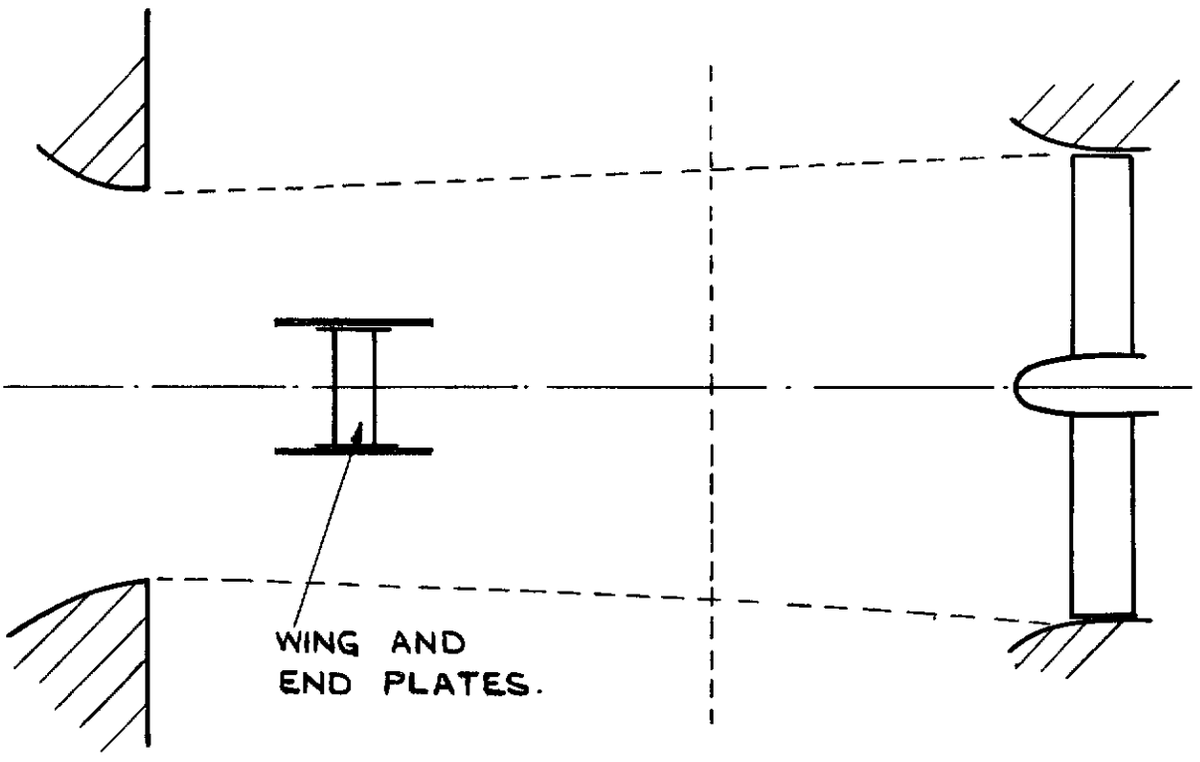

SIDE ELEVATION OF WORKING SECTION.

(a) WORKING SECTION SHOWING WING WITH TWO END PLATES IN POSITION.

FIG 3 (a) ARRANGEMENT OF END PLATES.

FIG. 3b & 4

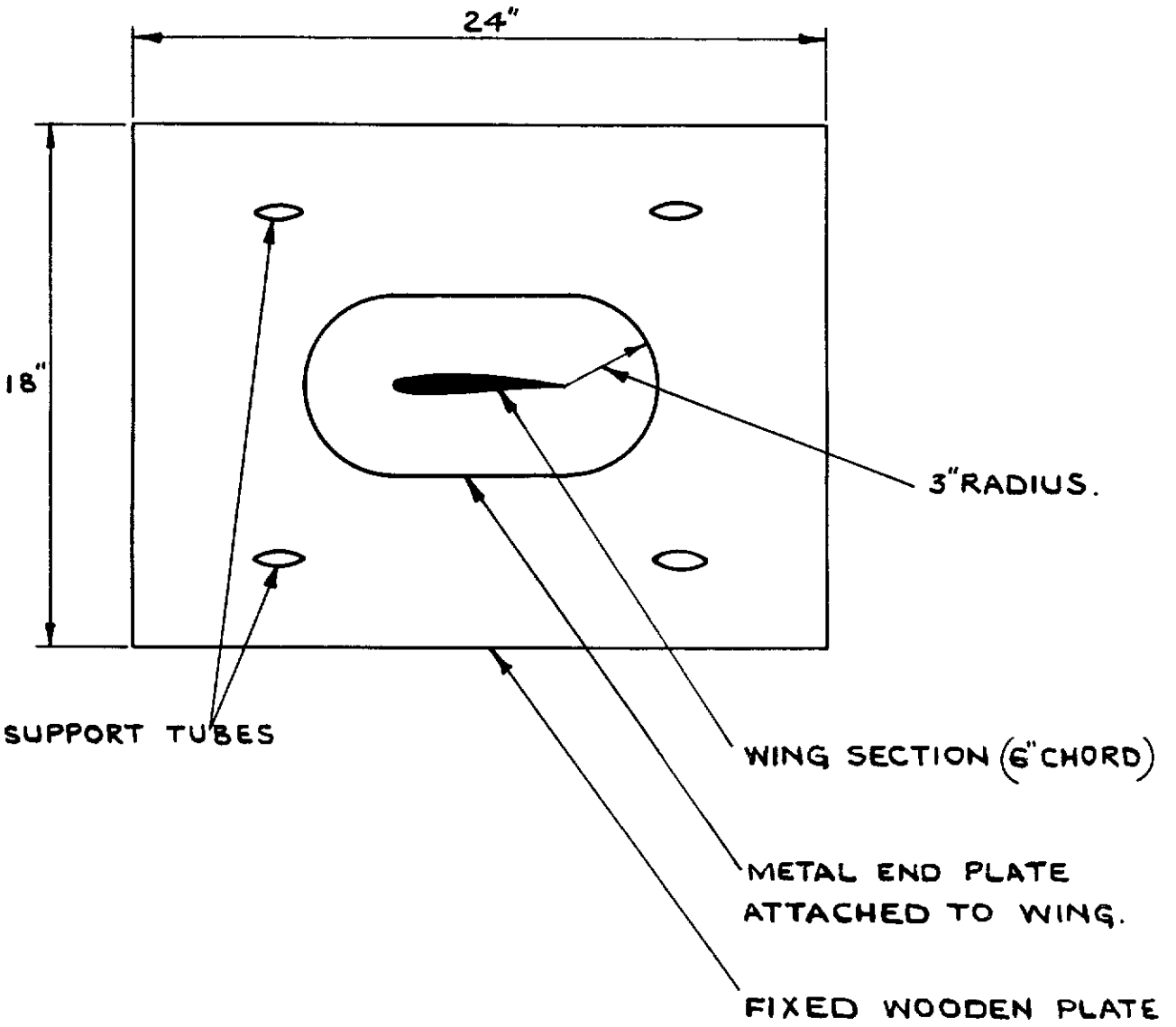

(b) DETAIL OF WOODEN AND METAL END PLATE.

FIG 3b. ARRANGEMENT OF END PLATES.

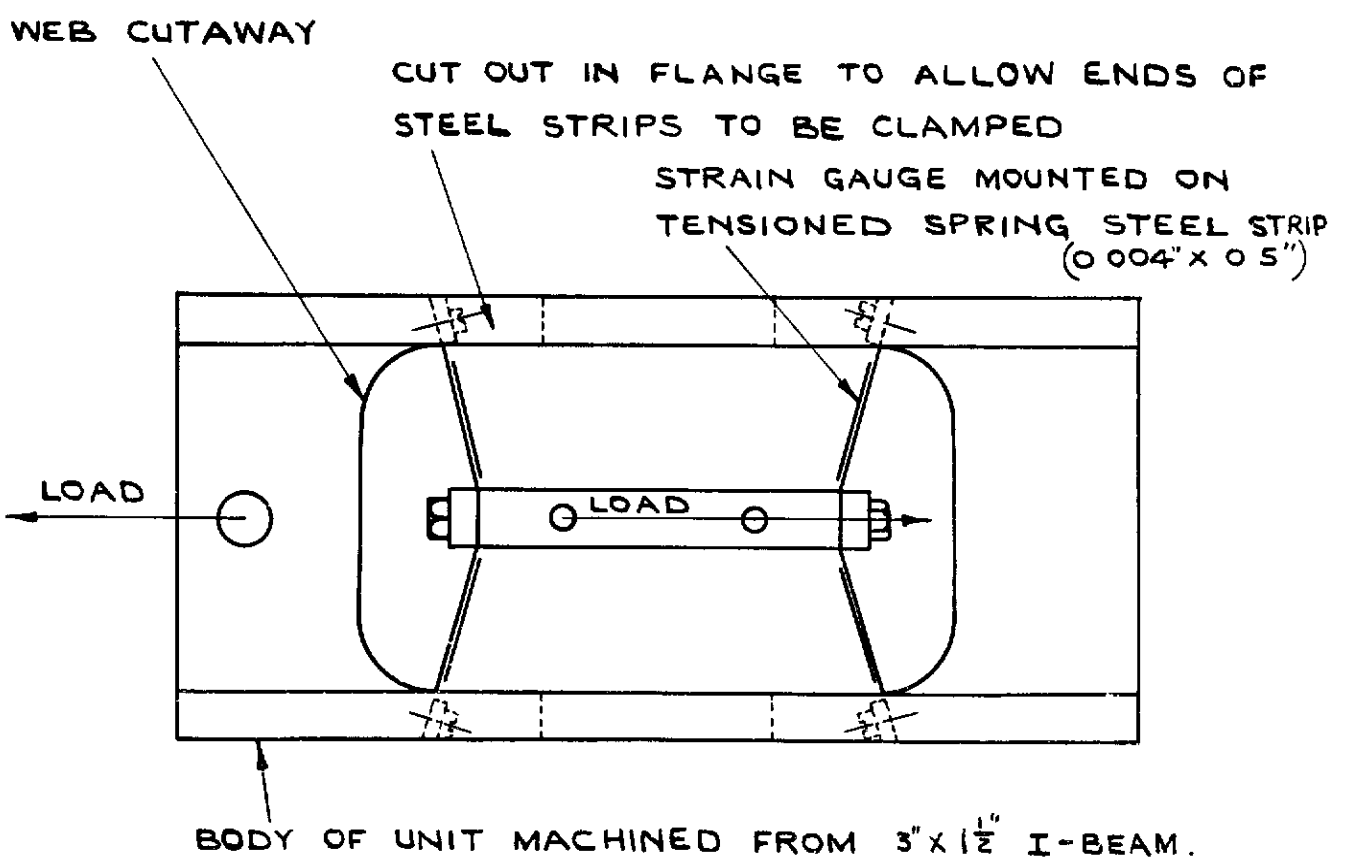

FIG. 4. FORCE MEASURING UNIT.

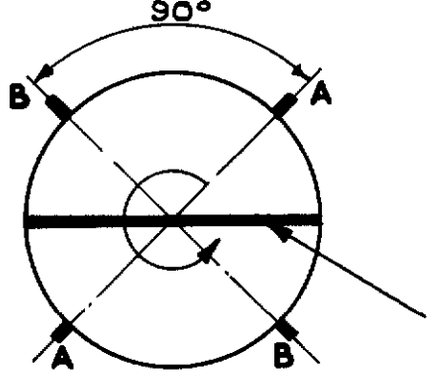

FIG. 5 & 6 (a b c)

WHEATSTONE'S BRIDGE OUTPUT SUPPLIED TO EITHER BRUSHES A-A OR B-B.

INSULATION BETWEEN 2 SEGMENTS OF COMMUTATOR.

SECTION ACROSS CENTRE OF COMMUTATOR

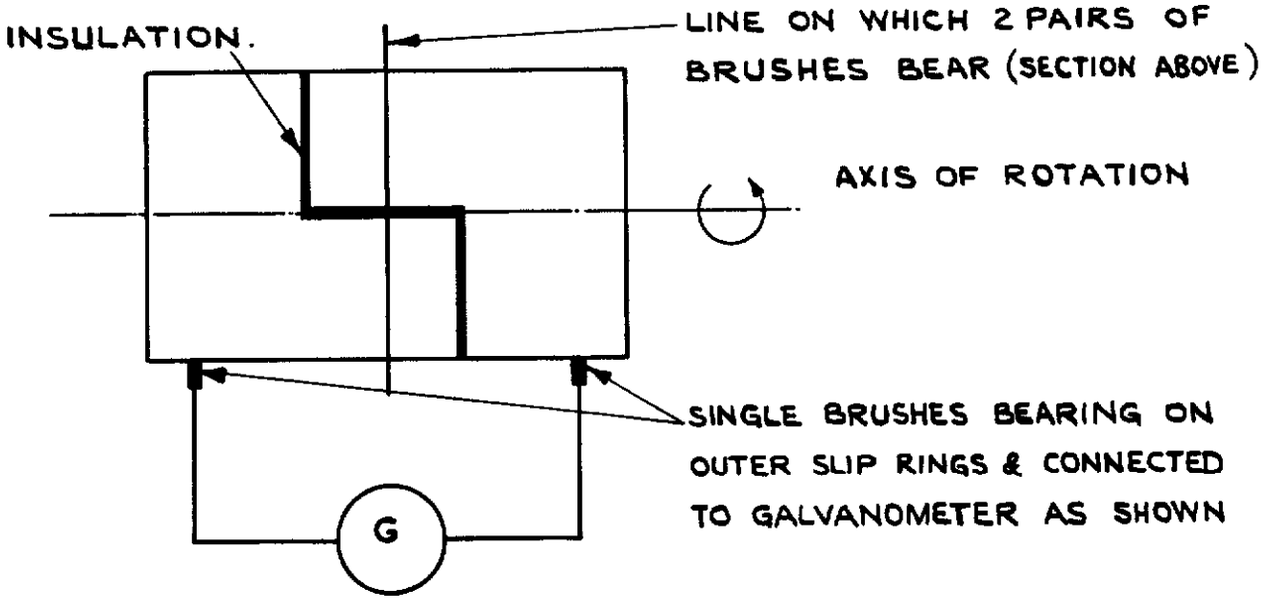

FIG. 5. THE COMMUTATOR & BRUSH ARRANGEMENT.

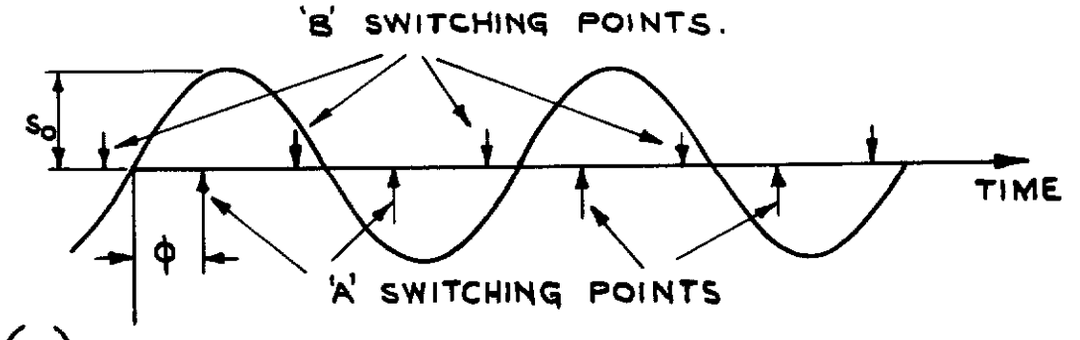

(a) SINE WAVE SIGNAL & SWITCHING POINTS.

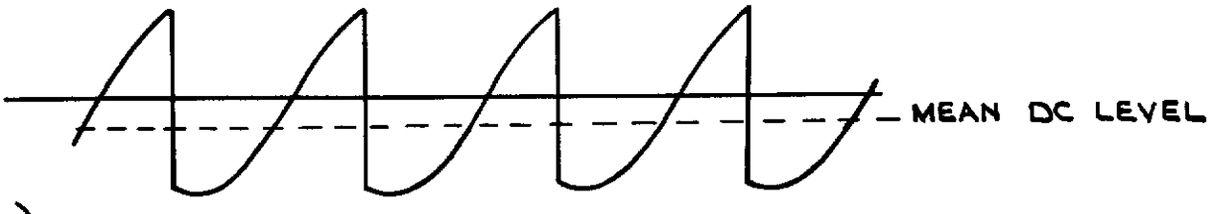

(b) SIGNAL SWITCHED AT A-A.

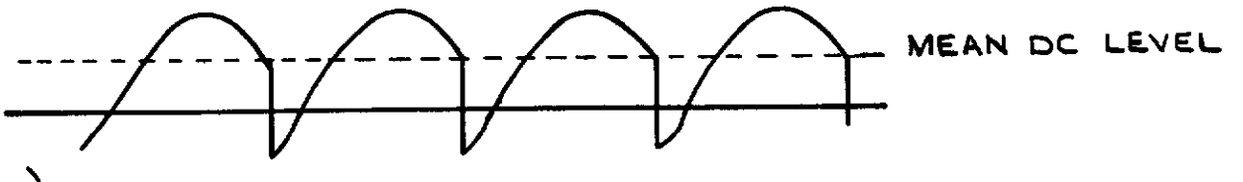

(c) SIGNAL SWITCHED AT B-B.

FIG. 6 (a b c.) GAUGE OUTPUT SIGNAL AND SWITCHING.

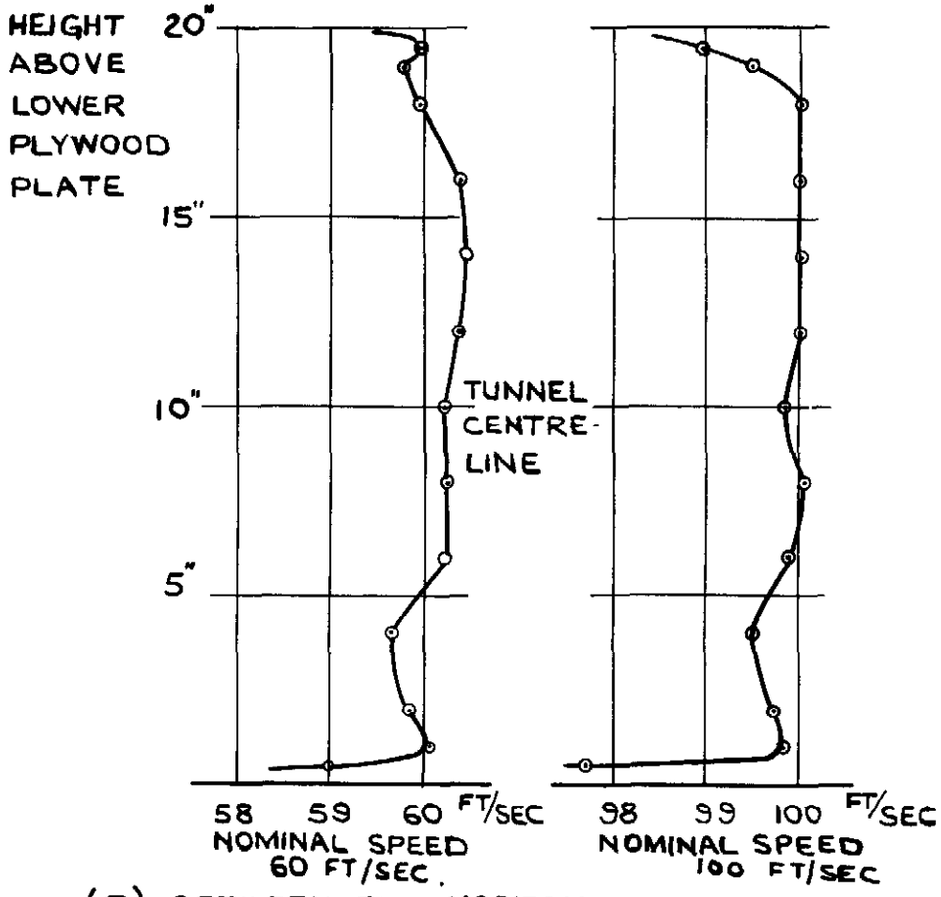

(a) BETWEEN TWO HORIZONTAL PLYWOOD PLATES 20 INCHES APART.

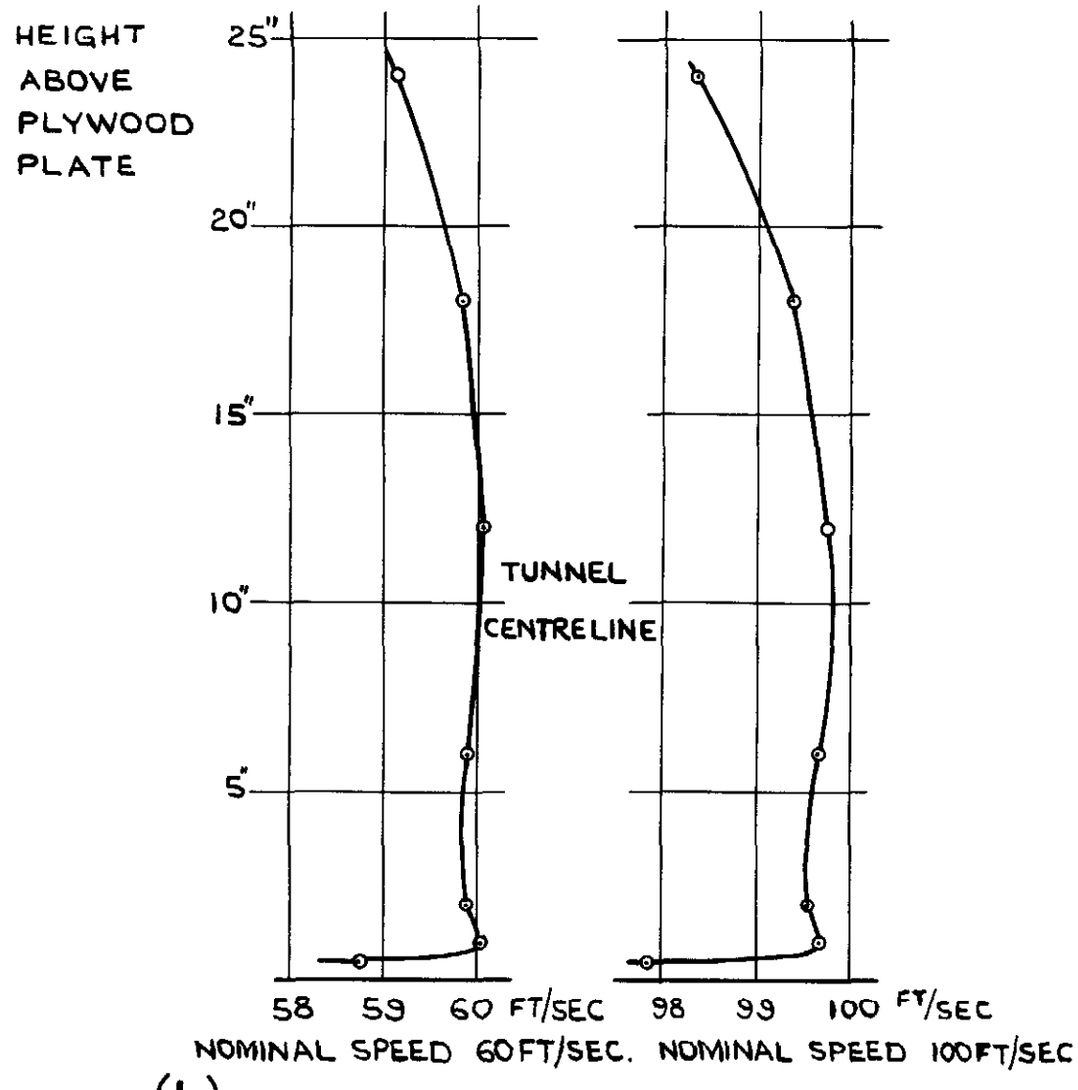

(b) ABOVE SINGLE HORIZONTAL PLYWOOD PLATE

FIG 7 (a & b) VELOCITY TRAVERSES ON MODEL SPANWISE CENTRE LINE.

FIG. 8(a)

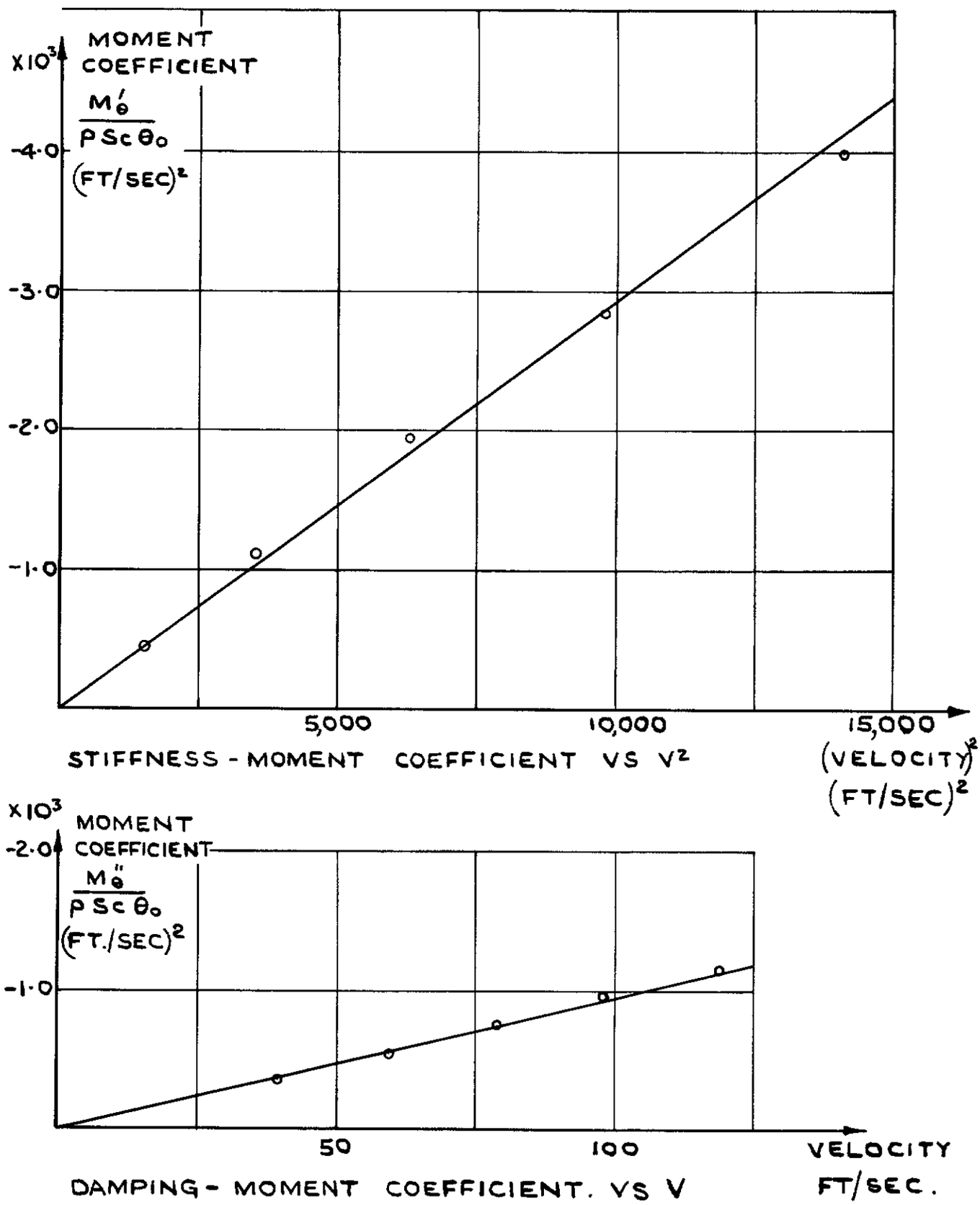

(a) WING ASPECT RATIO 2 PITCHING ABOUT ITS LEADING EDGE.

FIG. 8(a) MOMENT COEFFICIENTS VERSUS V & V².

FIG. 8(b)

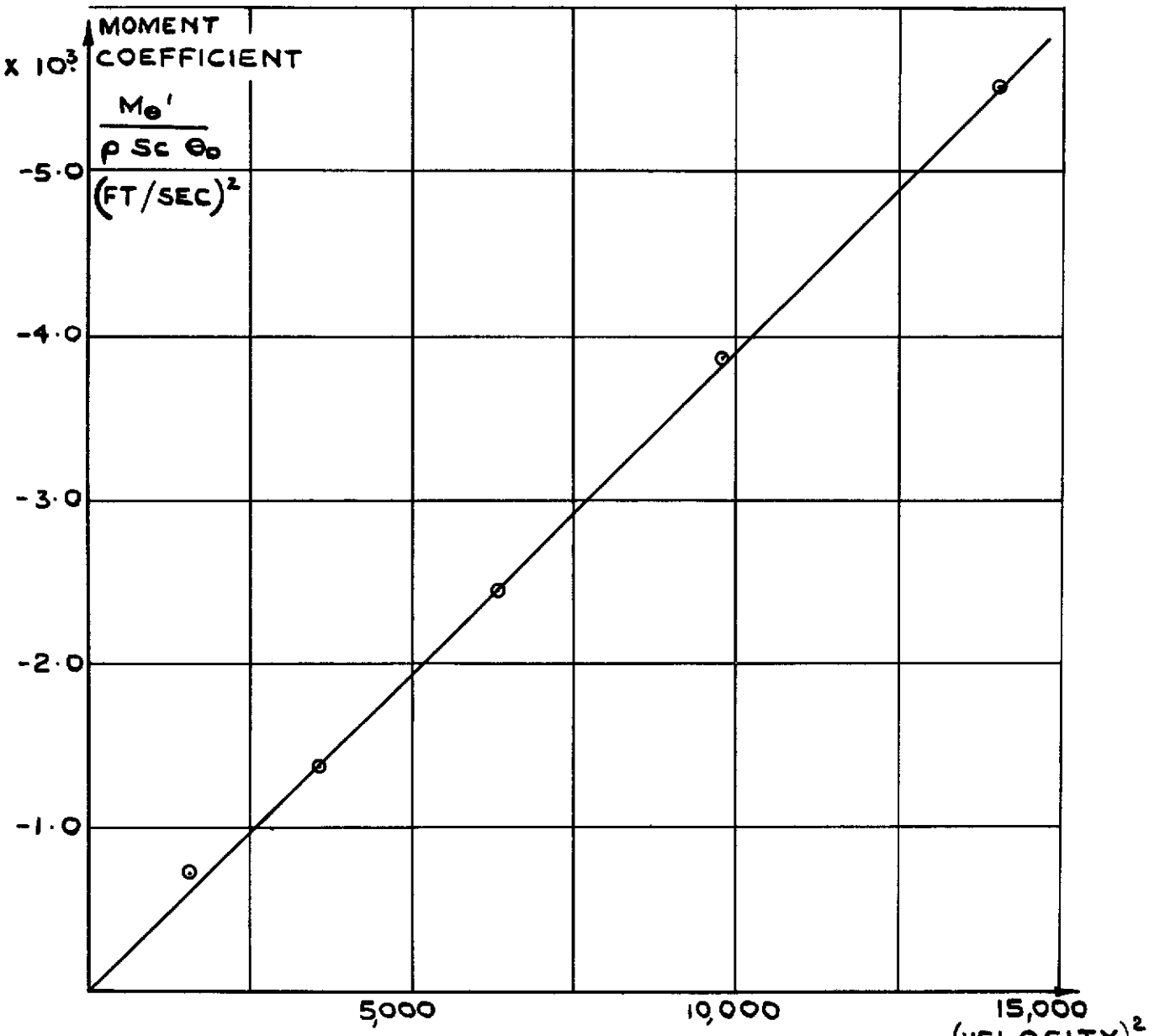

STIFFNESS-MOMENT COEFFICIENT VS V^2

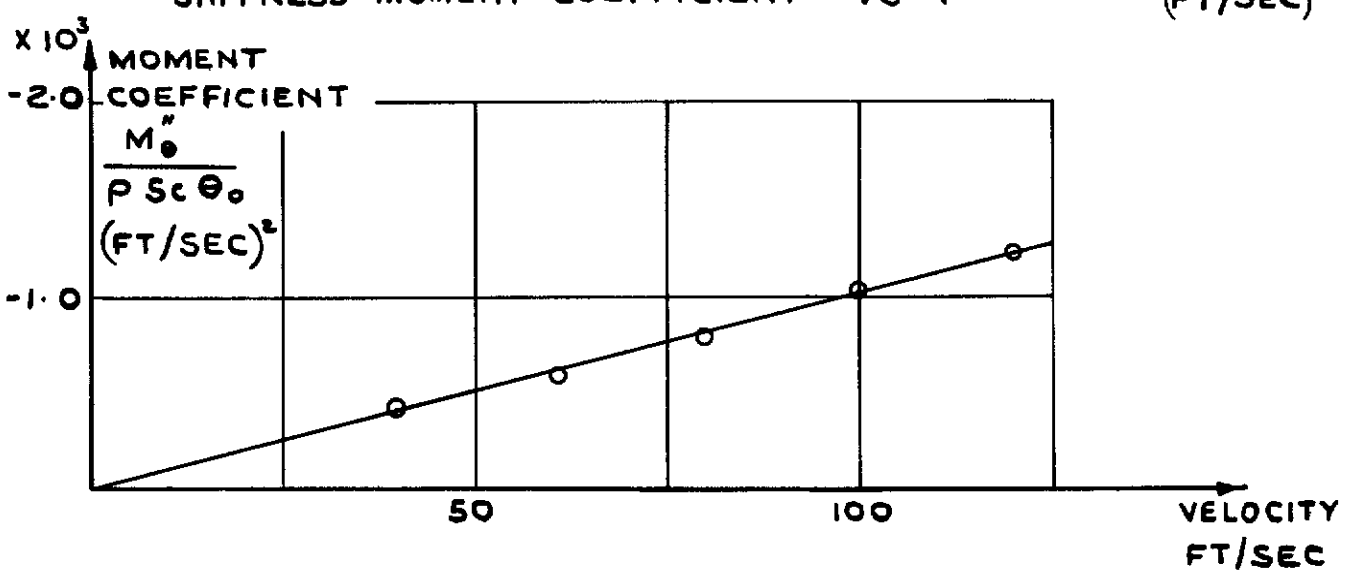

DAMPING-MOMENT COEFFICIENT VS V.

(b) WING ASPECT RATIO 3·25 PITCHING ABOUT ITS LEADING EDGE.

FIG. 8(b) MOMENT COEFFICIENTS VERSUS V & V^2.

FIG. 9(a & b)

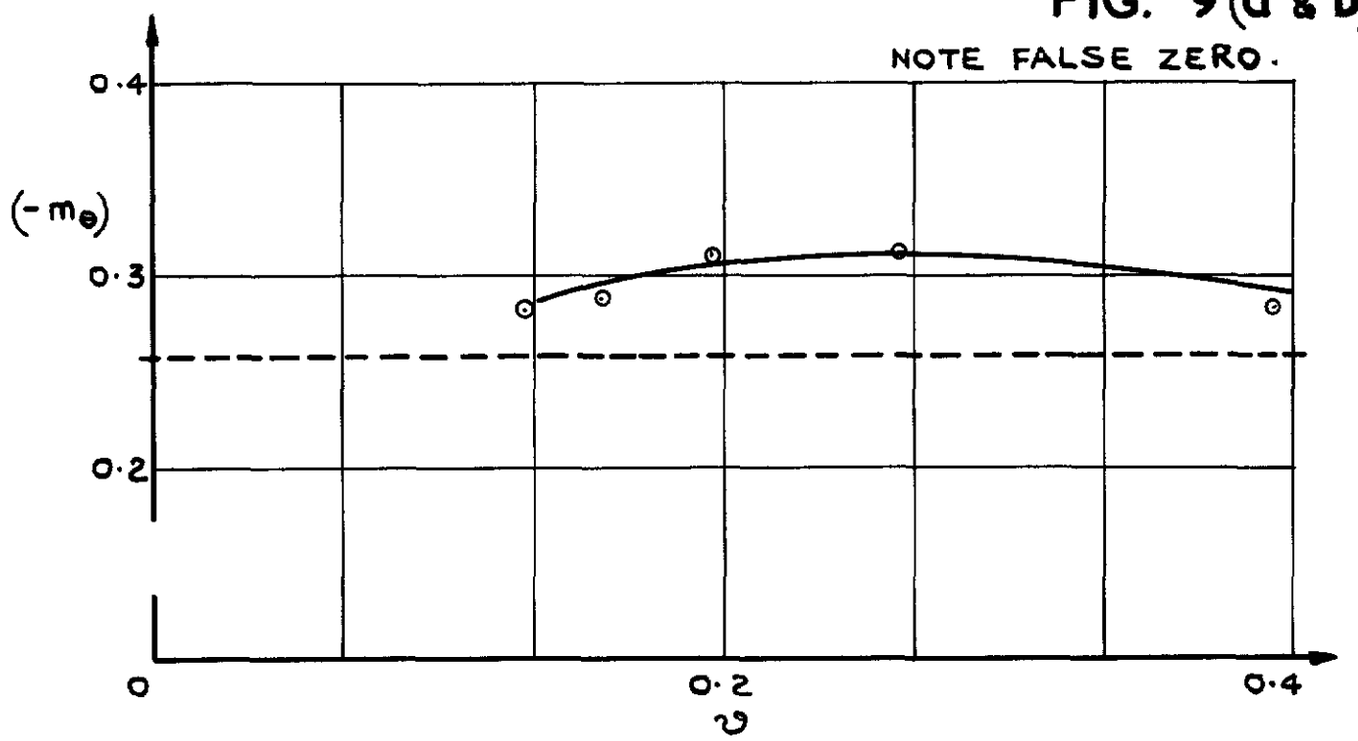

(a) ASPECT RATIO 2

EXPERIMENTAL RESULTS.

THEORY (SEE SECTION 7,3,2)

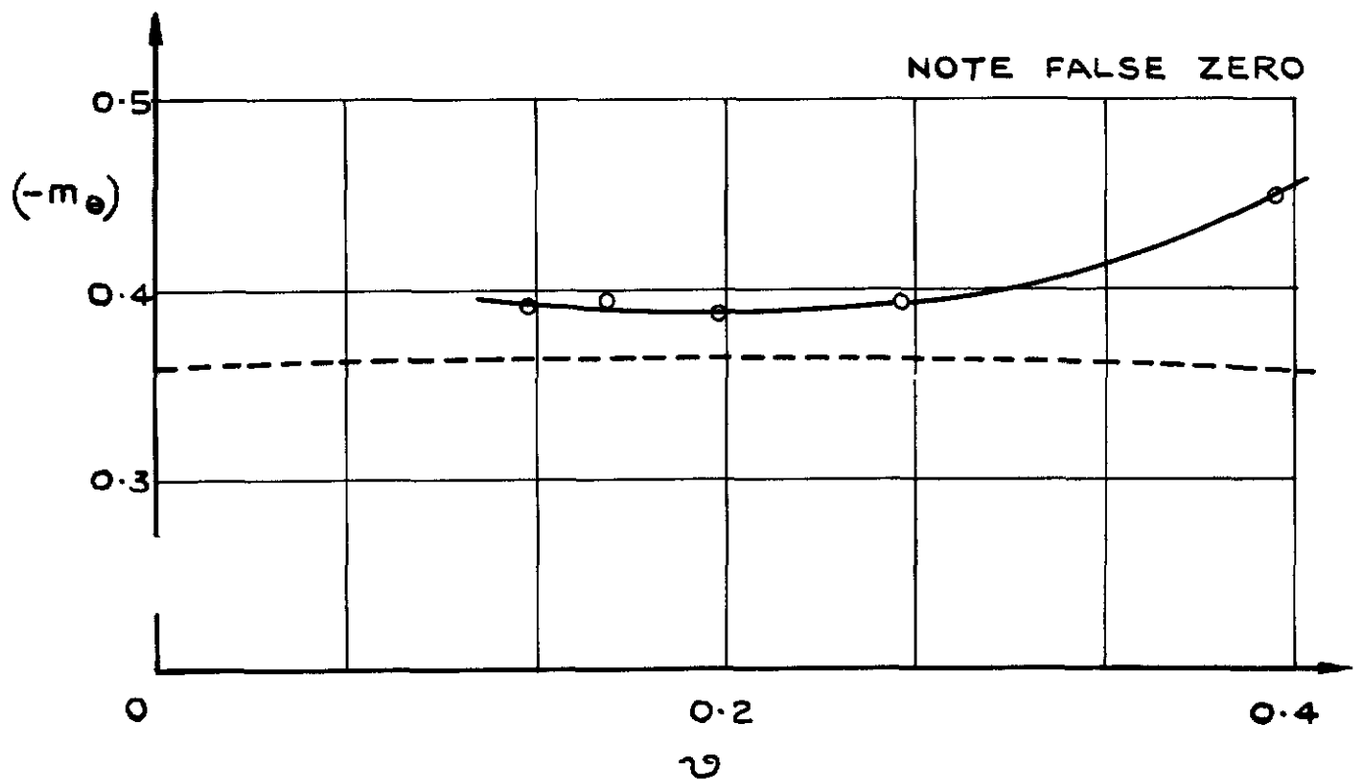

(b) ASPECT RATIO 3·25.

FIG. 9. (a & b). VARIATION OF THE STIFFNESS MOMENT DERIVATIVE $(-m_\theta)$ WITH FREQUENCY PARAMETER: PITCHING ABOUT LEADING EDGE.

FIG 9 (c - d)

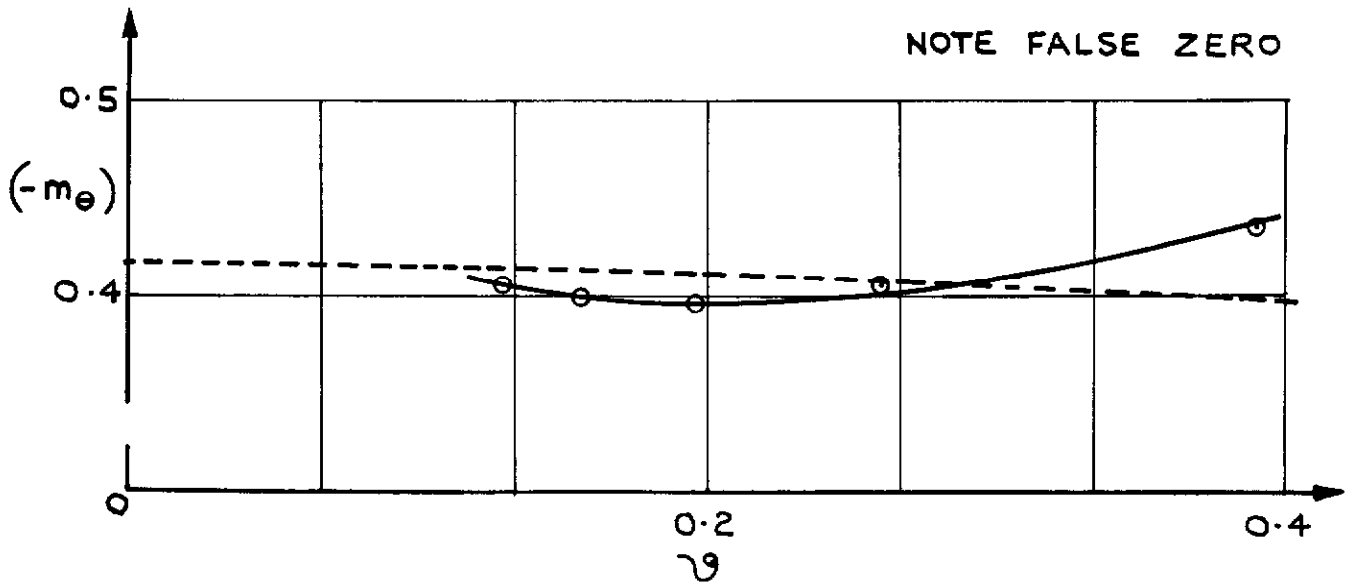

(C) ASPECT RATIO 4

—o— EXPERIMENTAL RESULTS.

------ THEORY (SEE SECTION 7,3,2)

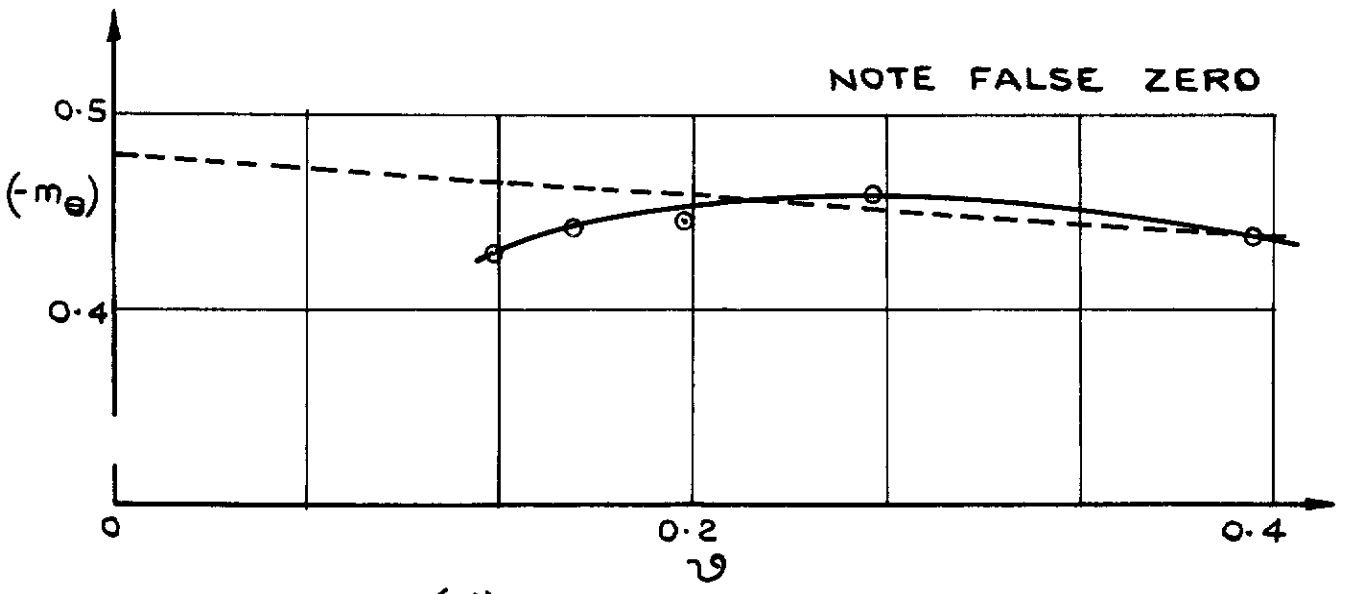

(d) ASPECT RATIO 5

FIG. 9 (c & d) VARIATION OF THE STIFFNESS MOMENT DERIVATIVE ($-m_\theta$) WITH FREQUENCY PARAMETER: PITCHING ABOUT LEADING EDGE.

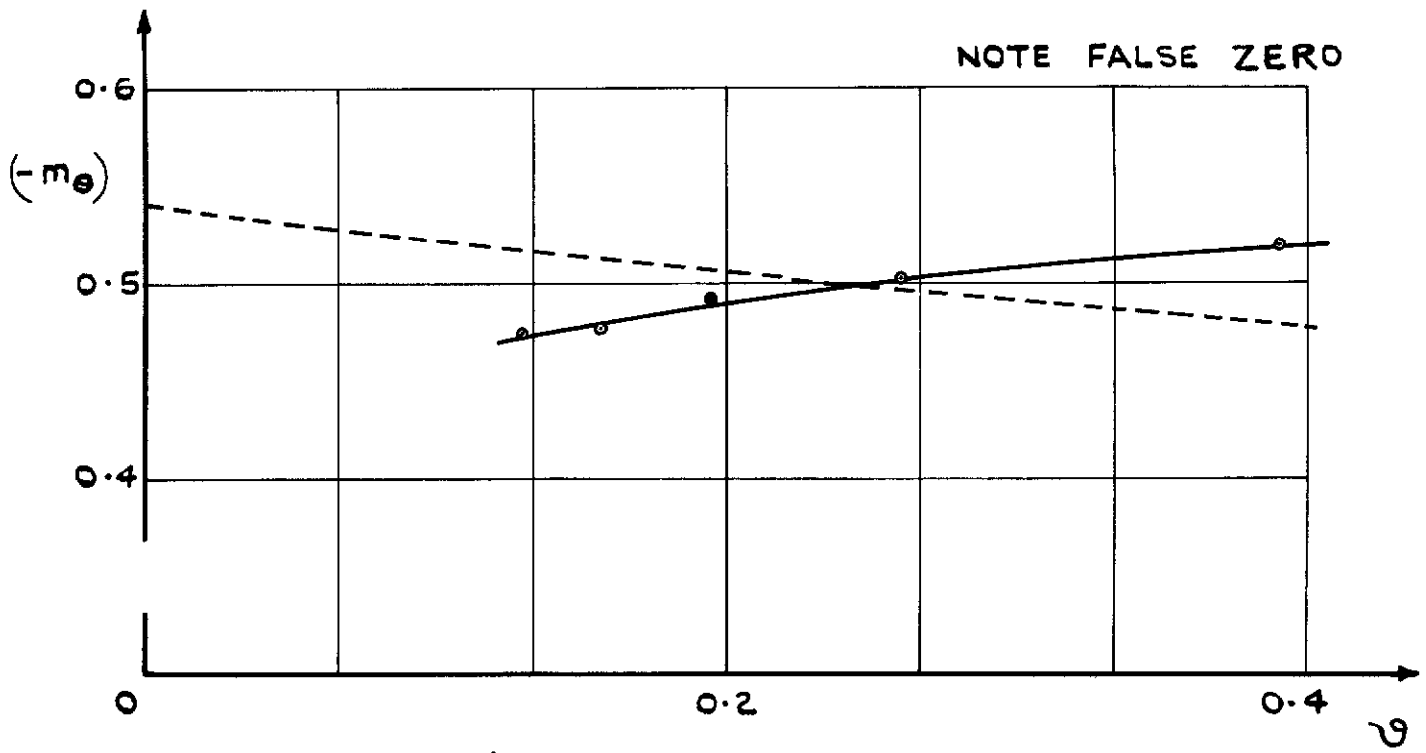

(e) ASPECT RATIO 6 5

—o— EXPERIMENTAL RESULTS
----- THEORY (SEE SECTION 7,3,2)

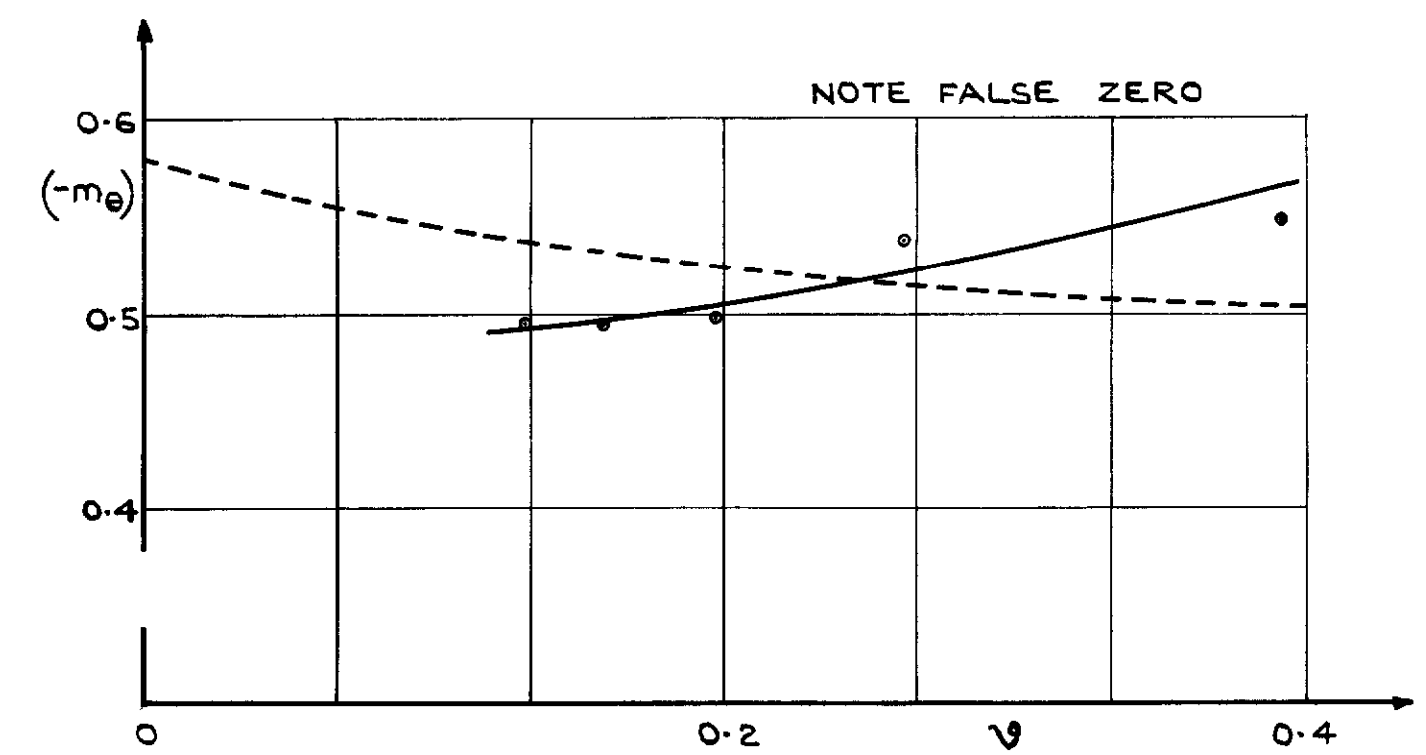

(f) ASPECT RATIO 8

FIG. 9 (e & f). VARIATION OF THE STIFFNESS MOMENT DERIVATIVE ($-m_\theta$) WITH FREQUENCY PARAMETER: PITCHING ABOUT LEADING EDGE.

FIG. 9 (g)

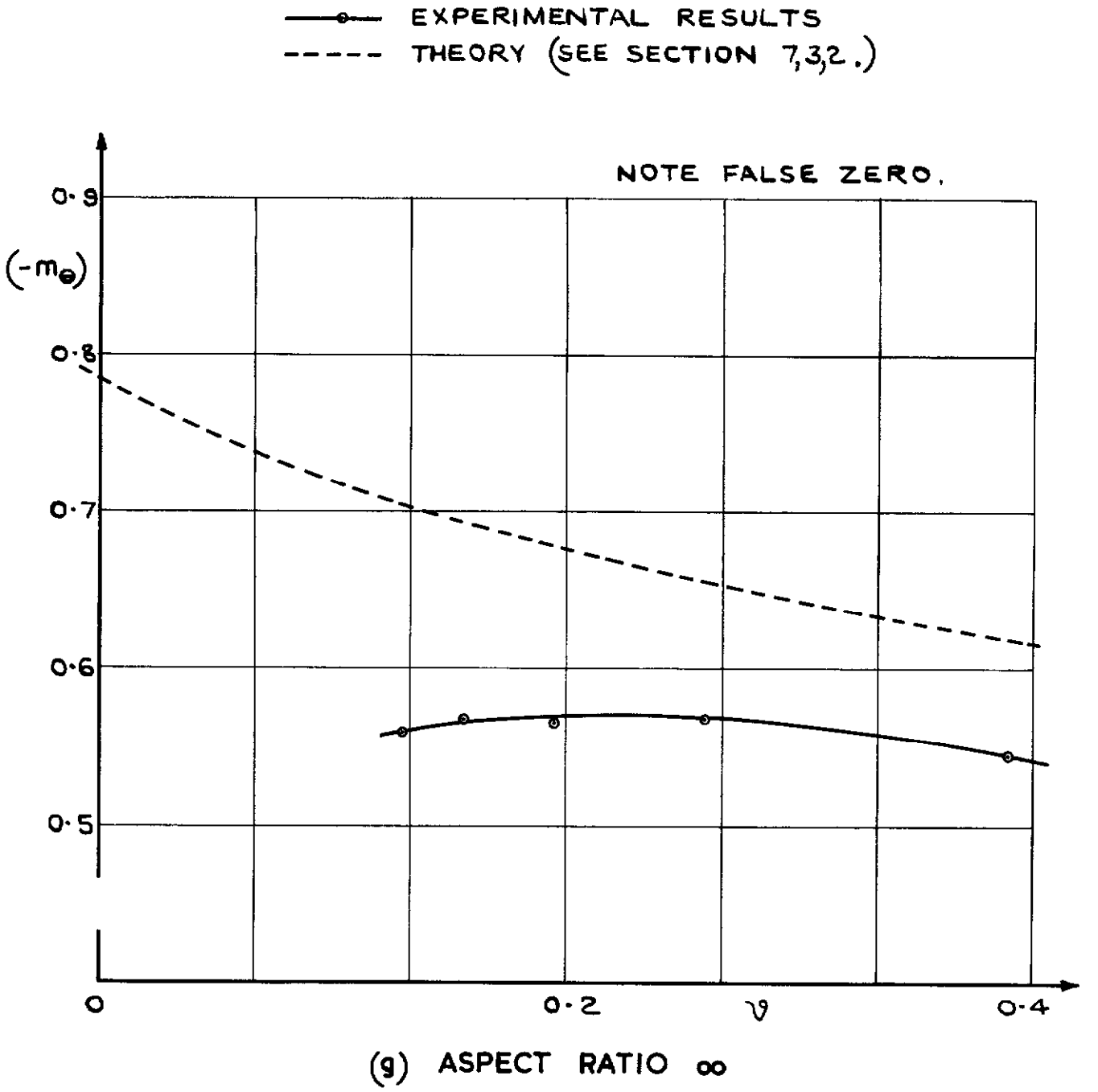

FIG 9(g) VARIATION OF THE STIFFNESS MOMENT DERIVATIVE (-me) WITH FREQUENCY PARAMETER: PITCHING ABOUT LEADING EDGE.

FIG. 10(a & b)

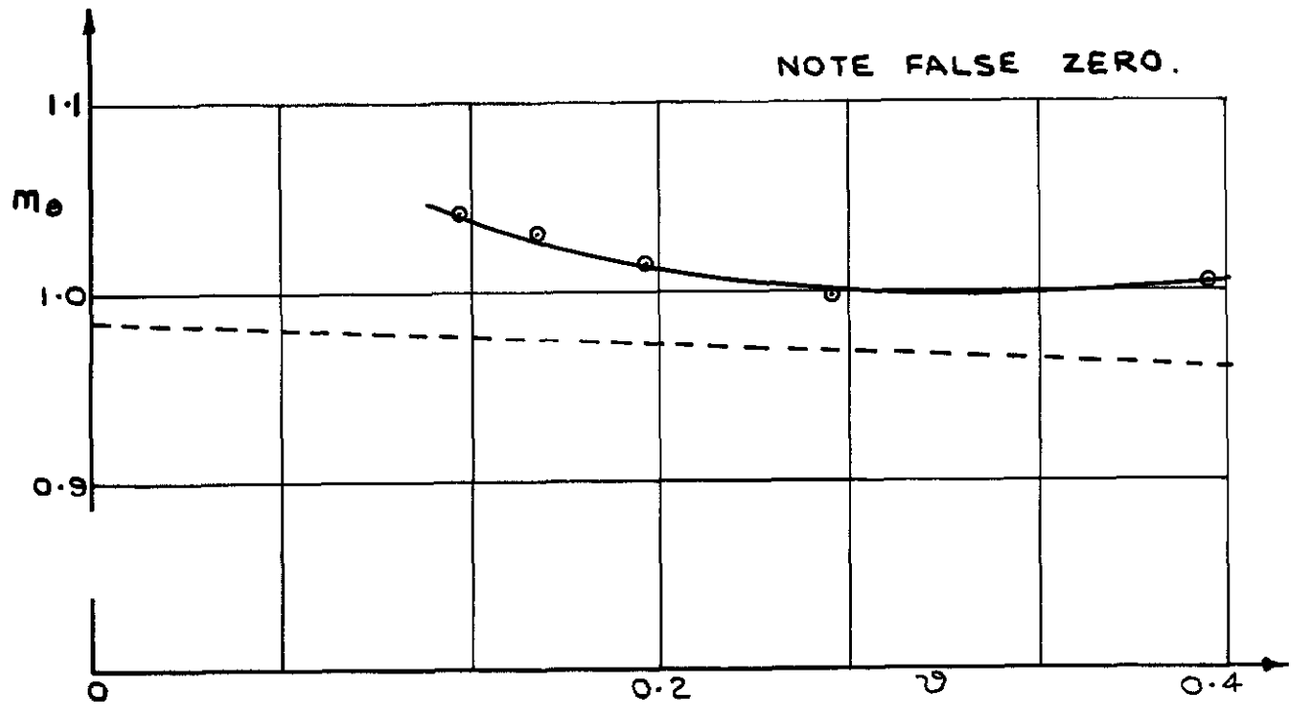

(a) ASPECT RATIO 2.

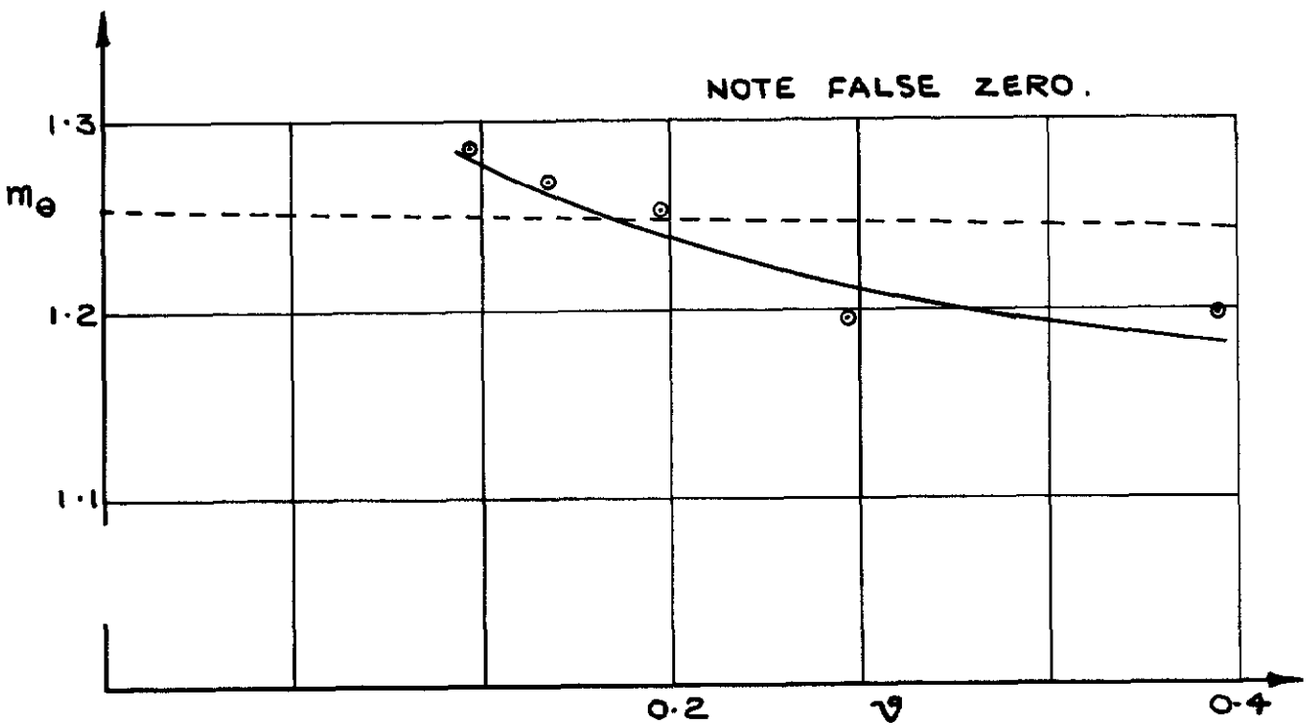

(b) ASPECT RATIO 3·25.

FIG. 10(a & b.) VARIATION OF THE STIFFNESS MOMENT DERIVATIVE m_θ WITH FREQUENCY PARAMETER: PITCHING ABOUT TRAILING EDGE.

FIG. 10(c & d)

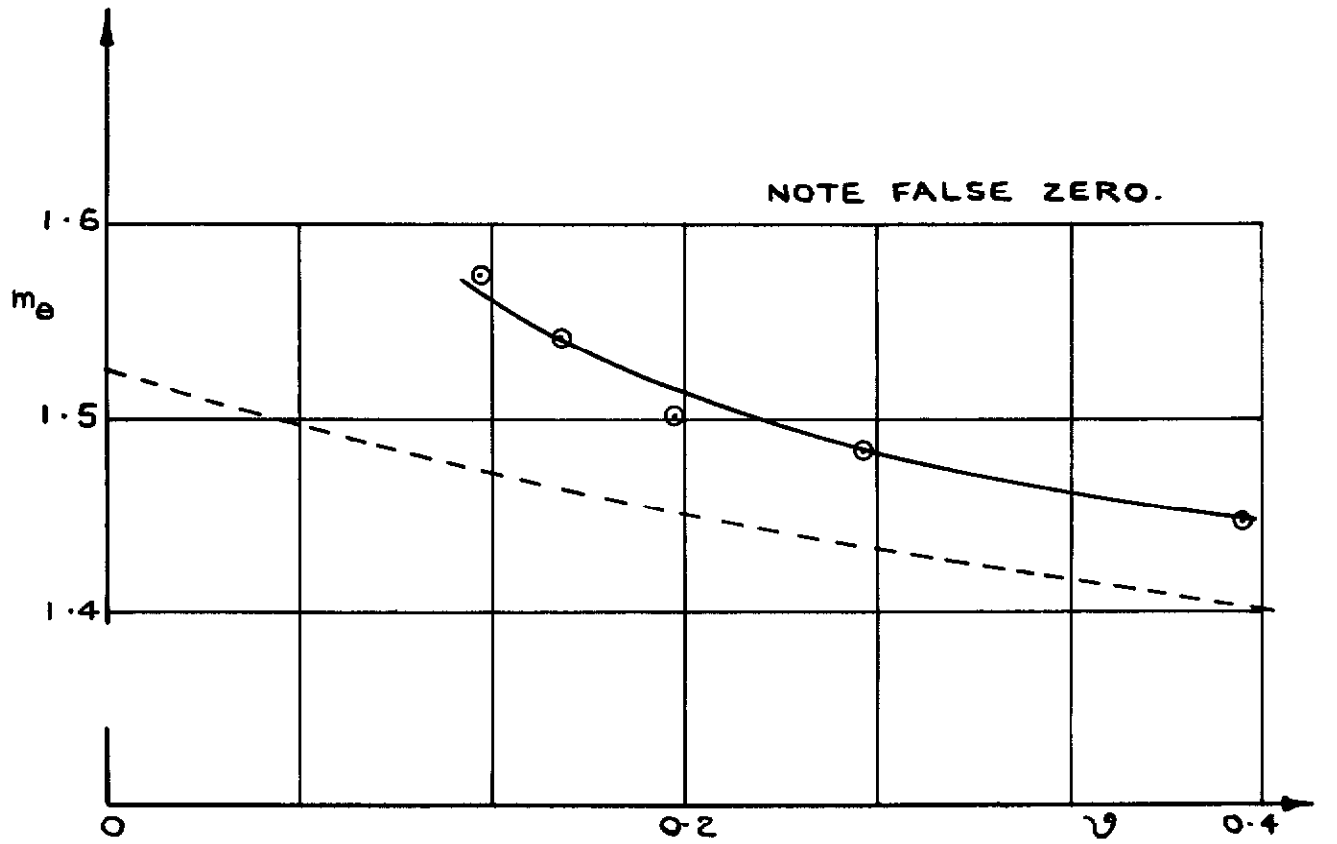

(c) ASPECT RATIO 5.

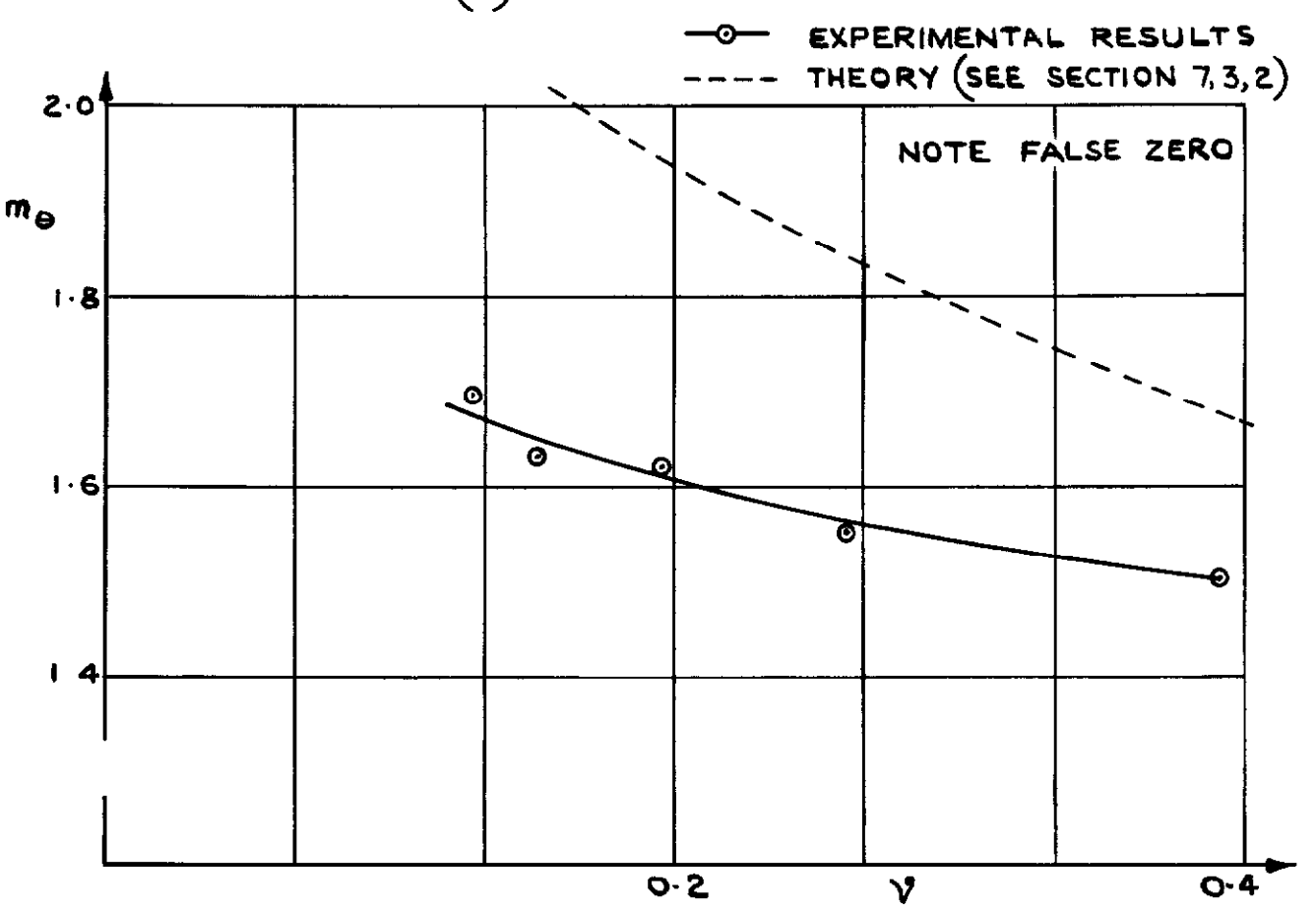

(d) ASPECT RATIO ∞.

FIG. 10(c & d) VARIATION OF THE STIFFNESS MOMENT DERIVATIVE m_e WITH FREQUENCY PARAMETER: PITCHING ABOUT TRAILING EDGE.

FIG. 11.

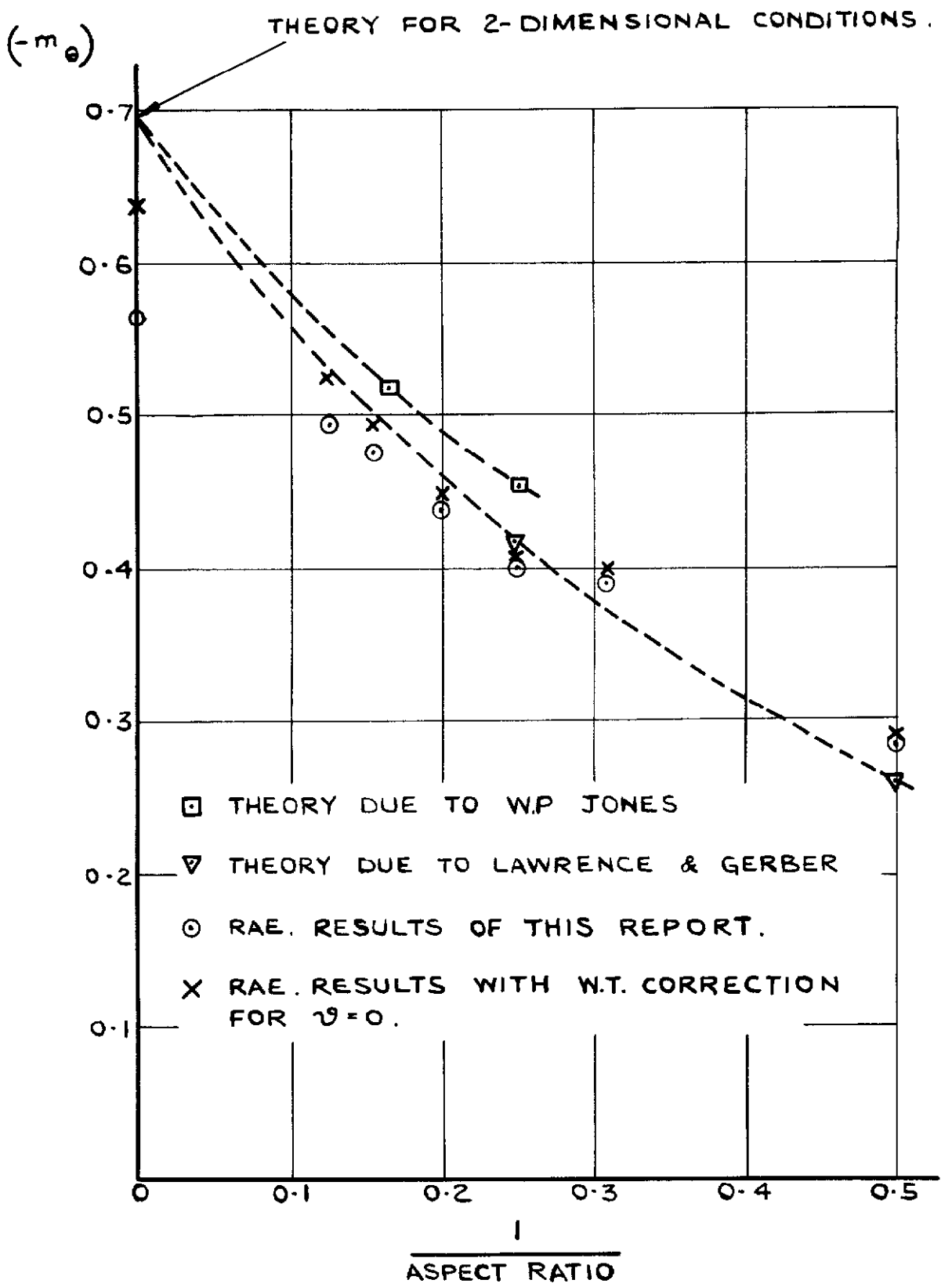

FIG. 11. VARIATION OF THE STIFFNESS MOMENT DERIVATIVE WITH $\frac{1}{\text{ASPECT RATIO}}$ FOR WINGS PITCHING ABOUT THEIR LEADING EDGES AT $\nu = 0{\cdot}15$.

FIG.12

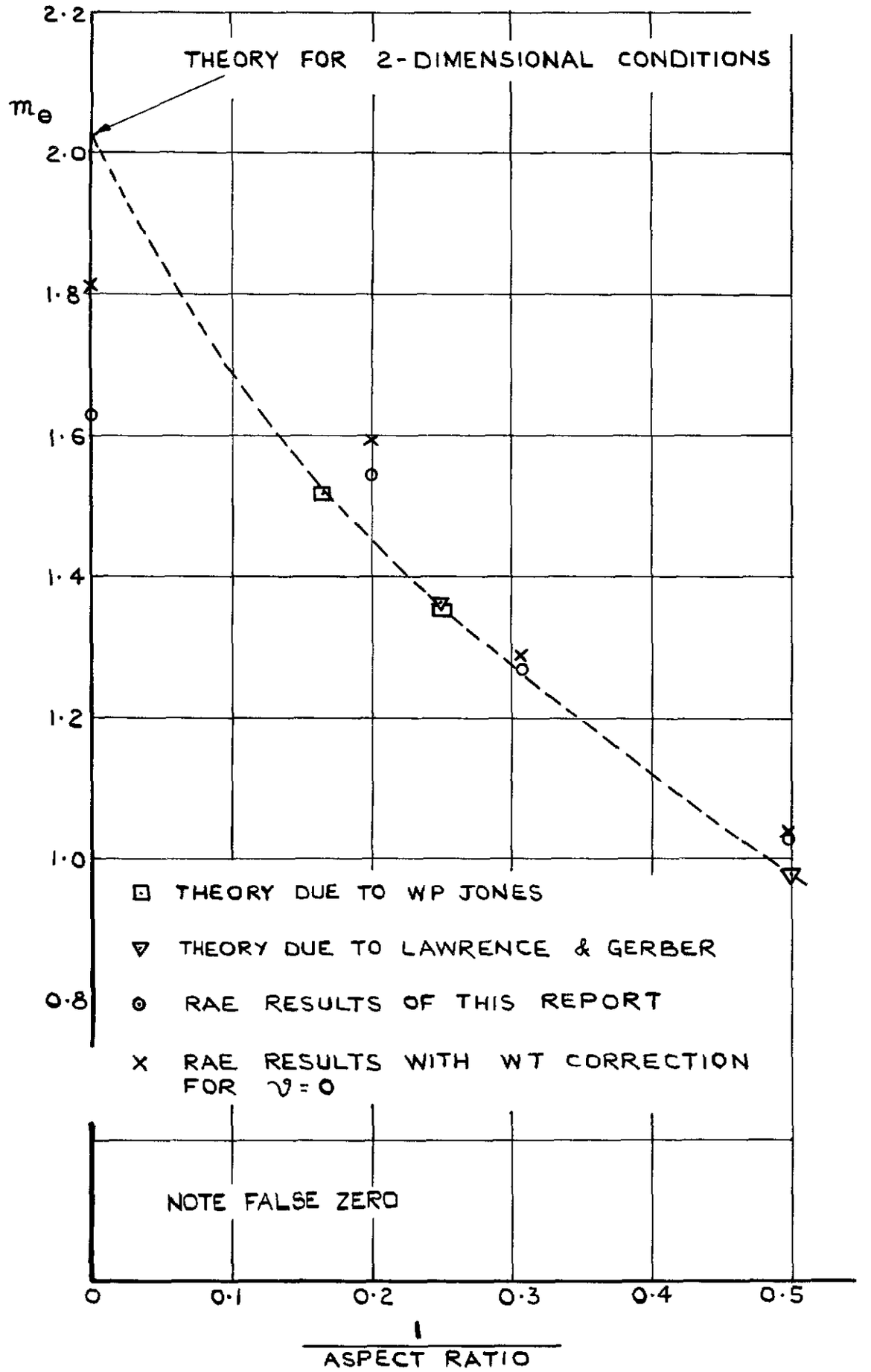

FIG. 12. VARIATION OF THE STIFFNESS MOMENT DERIVATIVE WITH $\frac{1}{\text{ASPECT RATIO}}$ FOR WINGS PITCHING ABOUT THEIR TRAILING EDGES

$\nu = 0 \cdot 15$

FIG. 13(a).

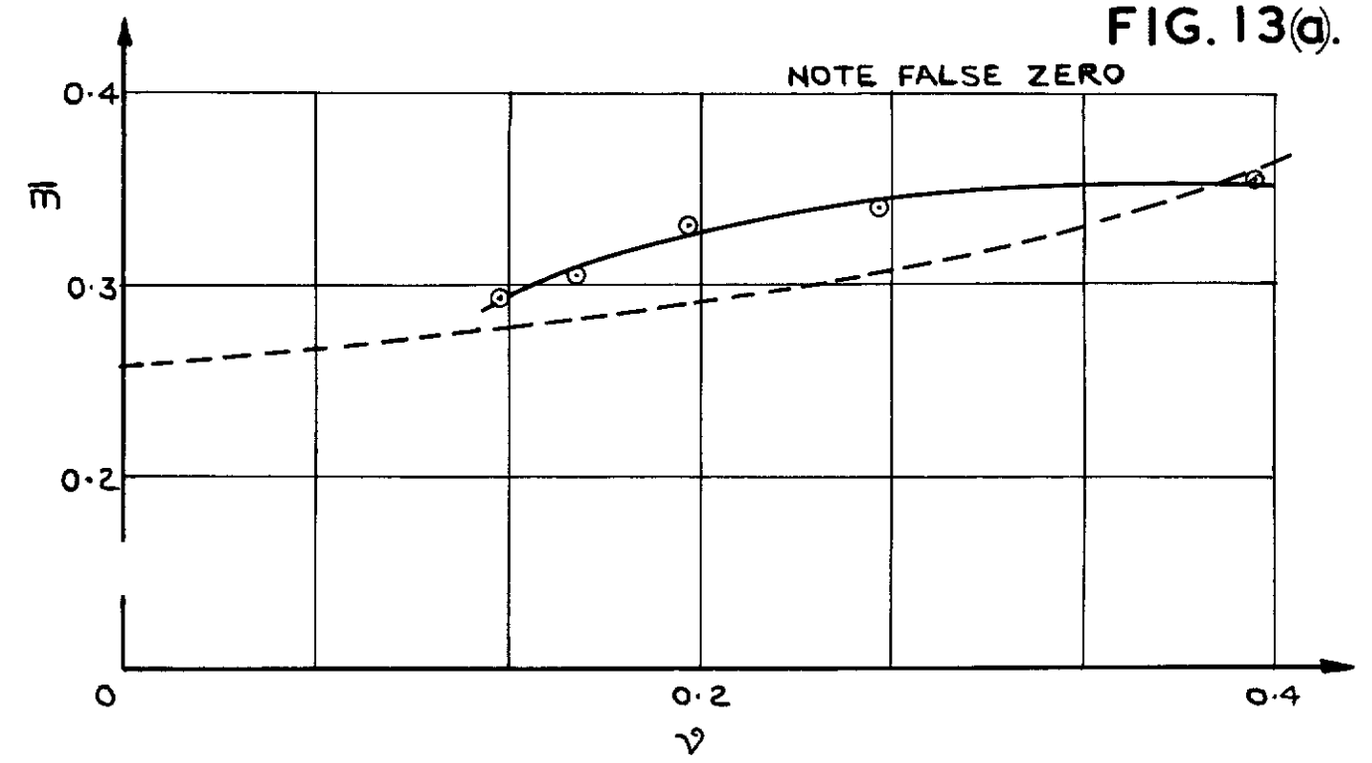

EXPERIMENTAL RESULTS

THEORY (SEE SECTION 7,3,2)

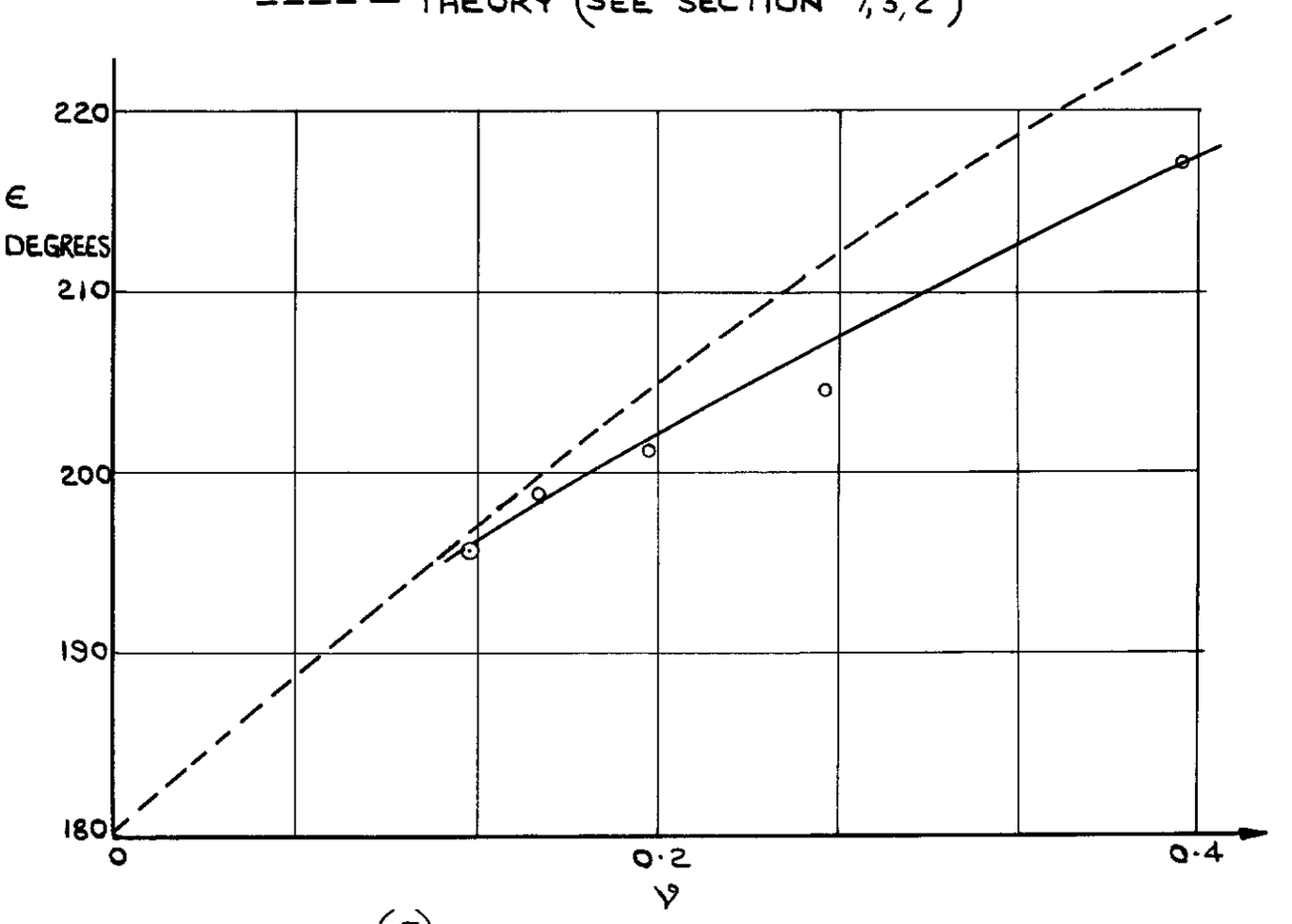

(a). ASPECT RATIO 2

FIG. 13(a). VARIATION OF RESULTANT MOMENT AND PHASE ANGLE WITH FREQUENCY PARAMETER : PITCHING ABOUT LEADING EDGE.

FIG. 13 (b)

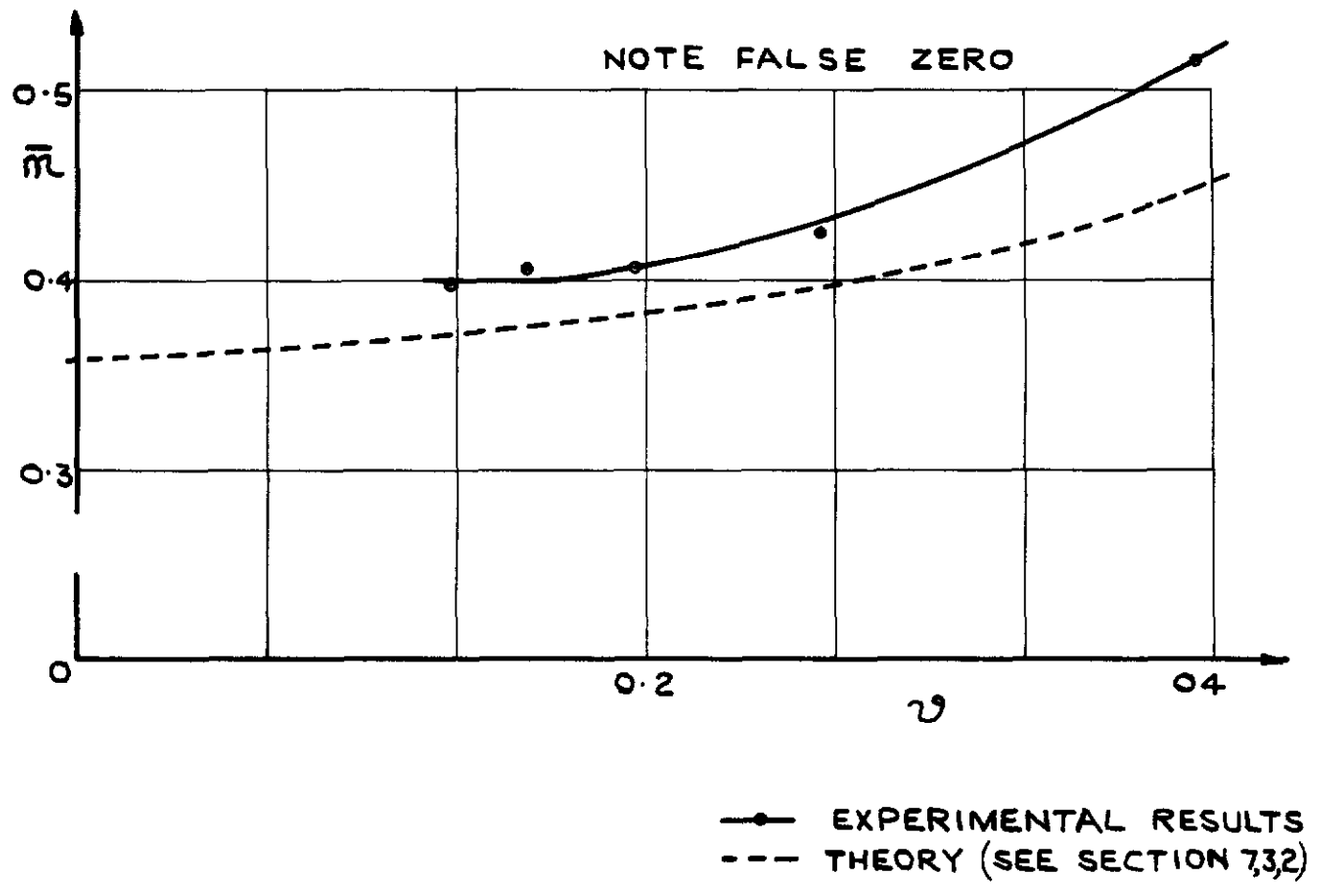

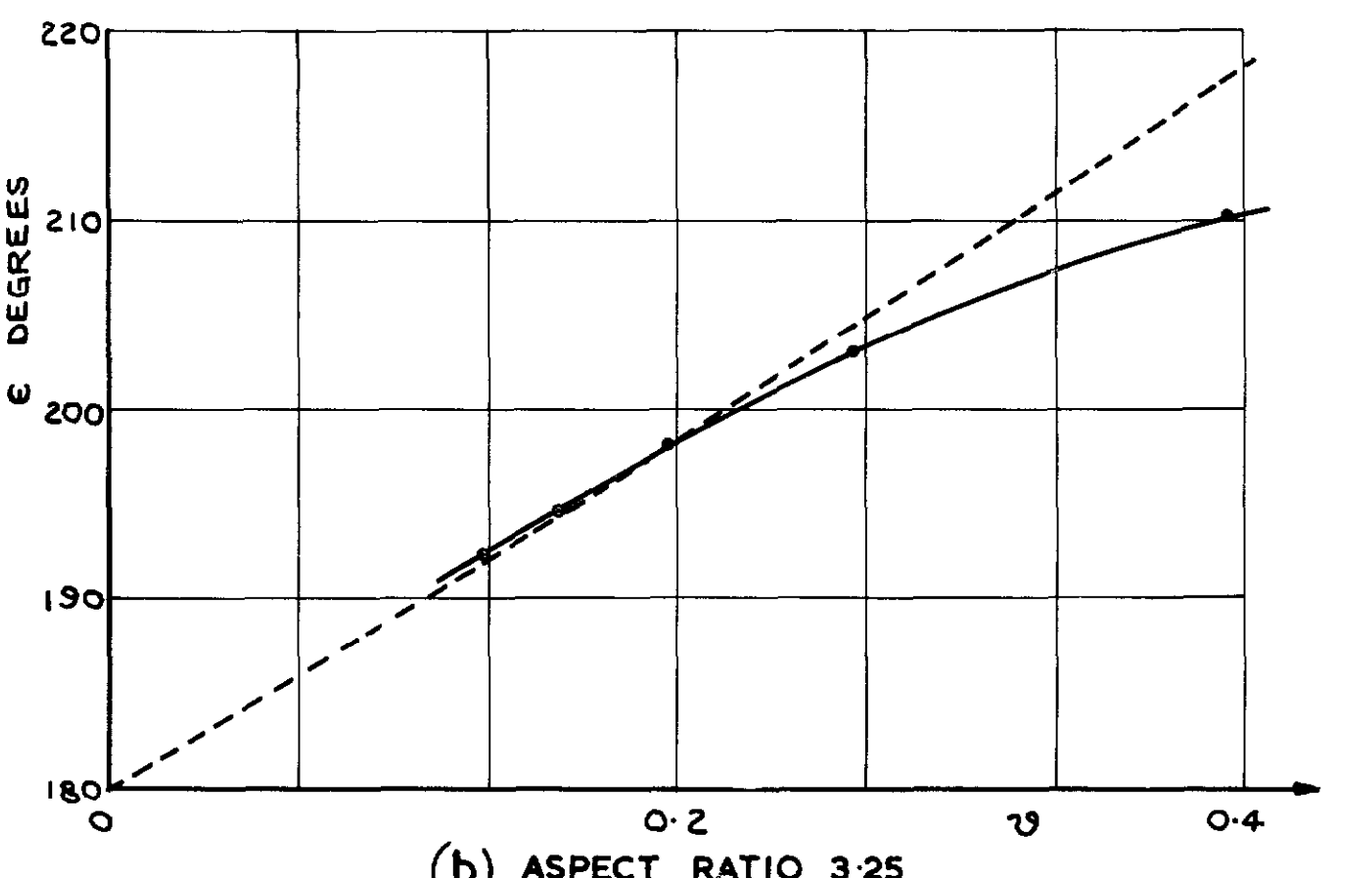

(b) ASPECT RATIO 3·25

FIG. 13 (b) VARIATION OF RESULTANT MOMENT AND PHASE ANGLE WITH FREQUENCY PARAMETER: PITCHING ABOUT LEADING EDGE.

FIG. 13 (c)

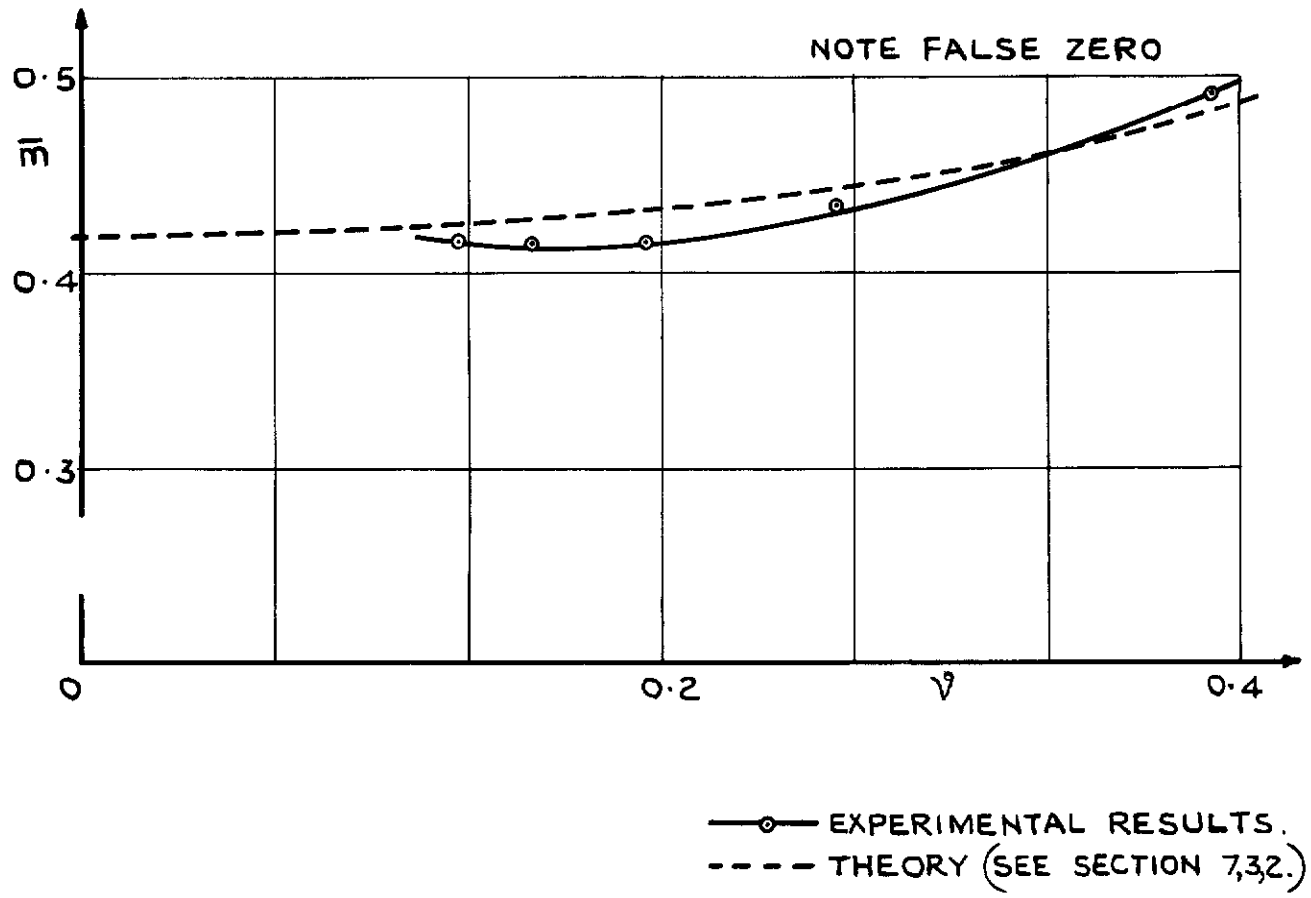

—o— EXPERIMENTAL RESULTS.
- - - - THEORY (SEE SECTION 7,3,2.)

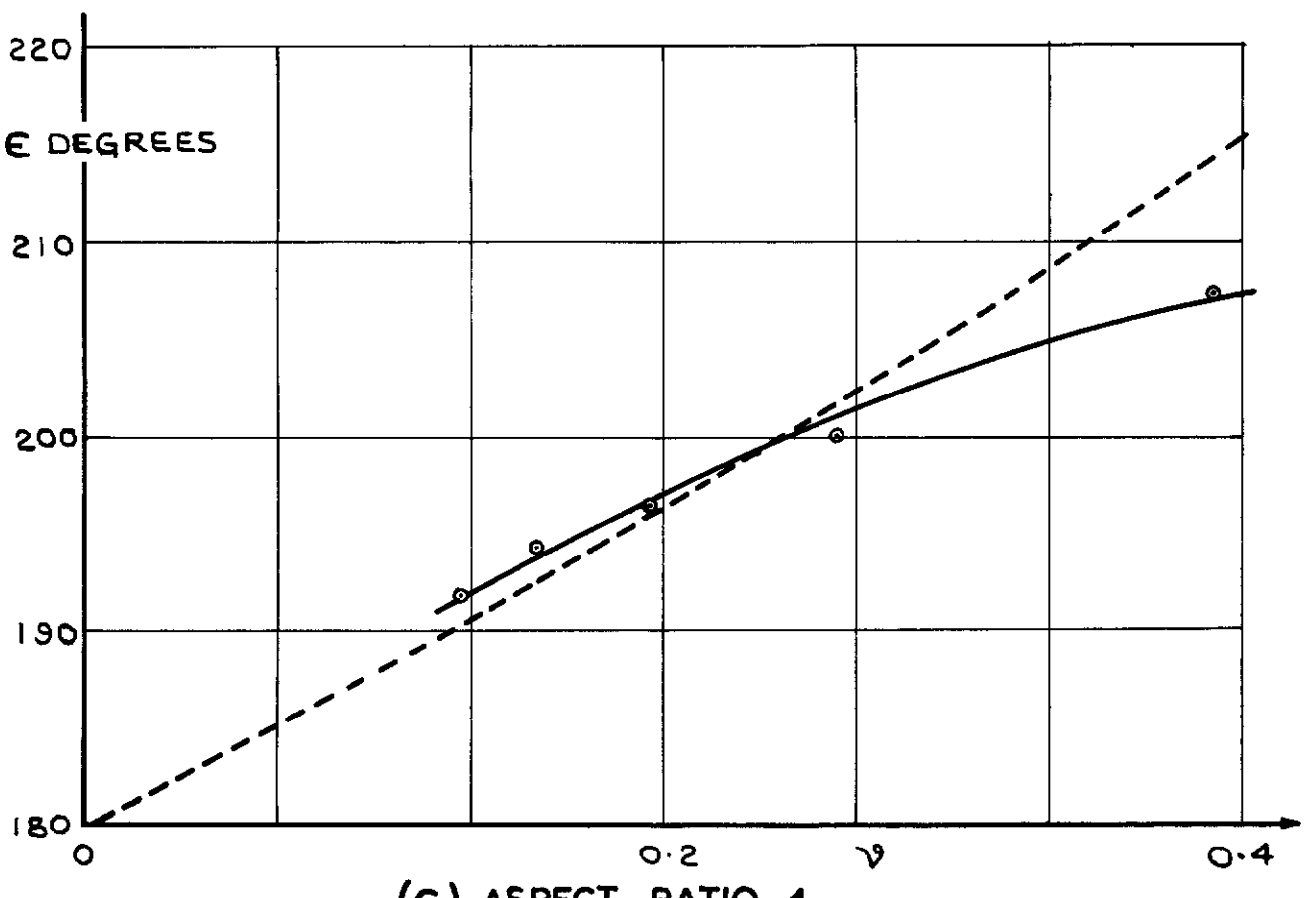

(c) ASPECT RATIO 4

FIG. 13 (c) VARIATION OF RESULTANT MOMENT AND PHASE ANGLE WITH FREQUENCY PARAMETER: PITCHING ABOUT LEADING EDGE.

FIG. 13.(d)

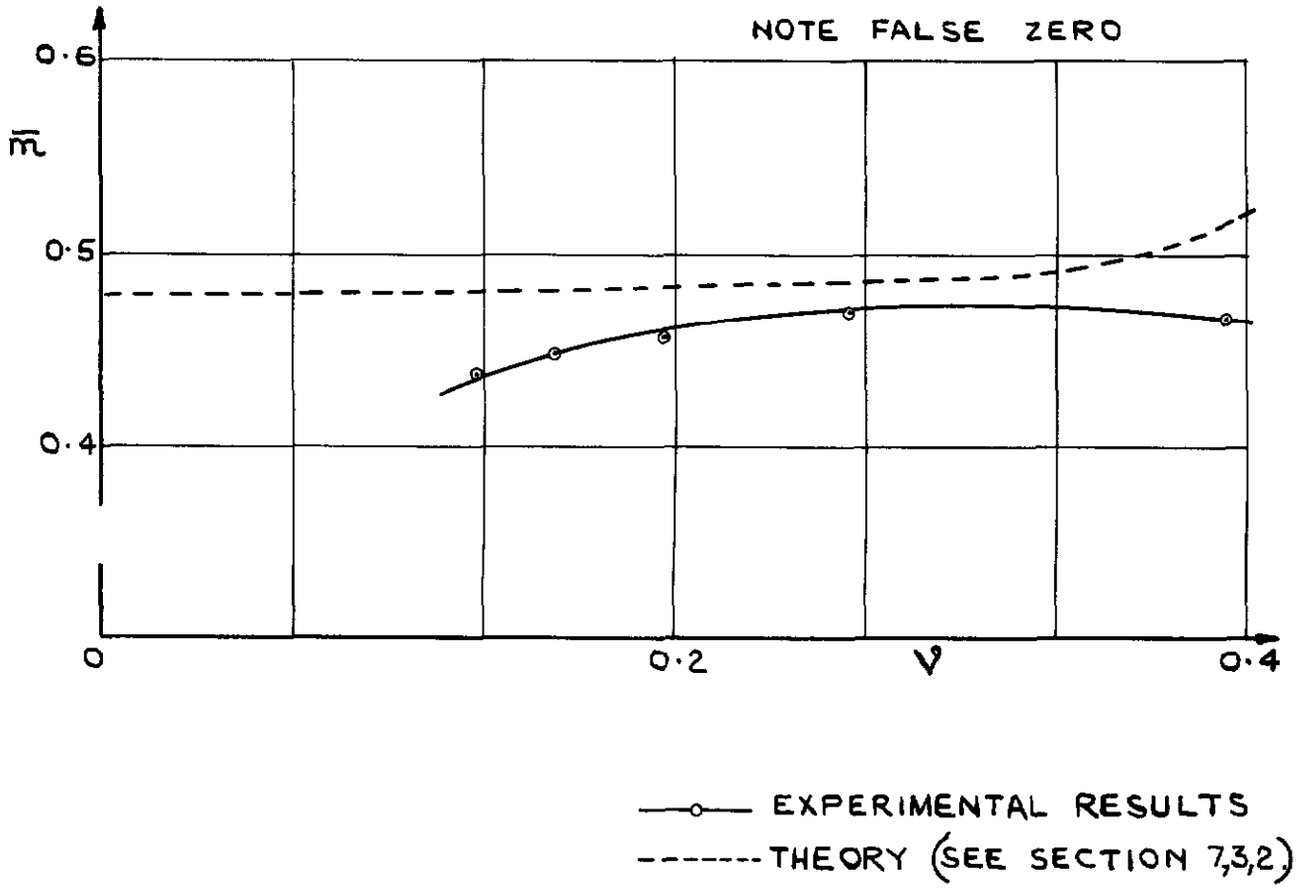

—o— EXPERIMENTAL RESULTS

------ THEORY (SEE SECTION 7,3,2.)

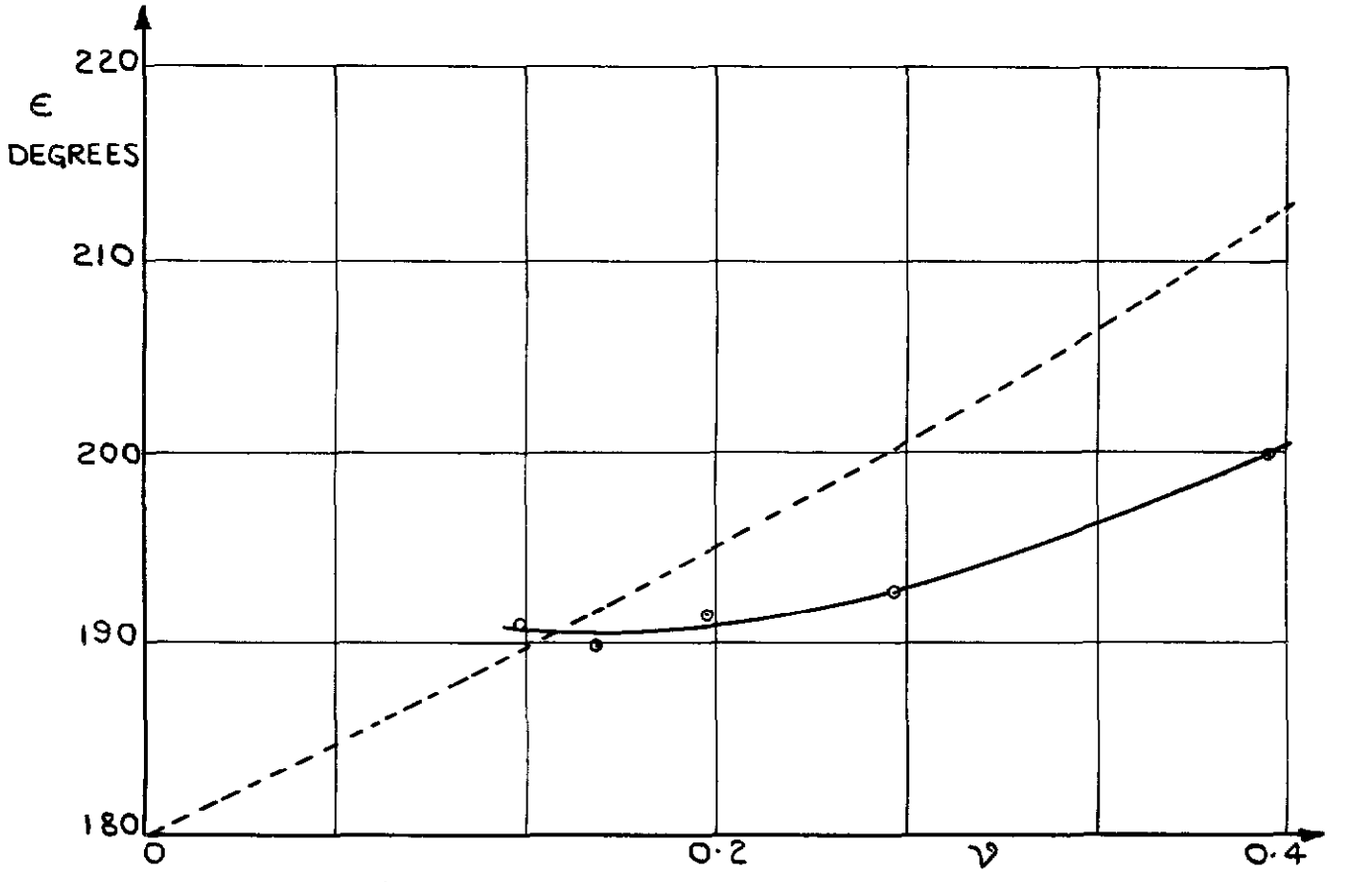

(d) ASPECT RATIO 5

FIG 13(d) VARIATION OF RESULTANT MOMENT & PHASE ANGLE WITH FREQUENCY PARAMETER: PITCHING ABOUT LEADING EDGE.

FIG. 13 (e)

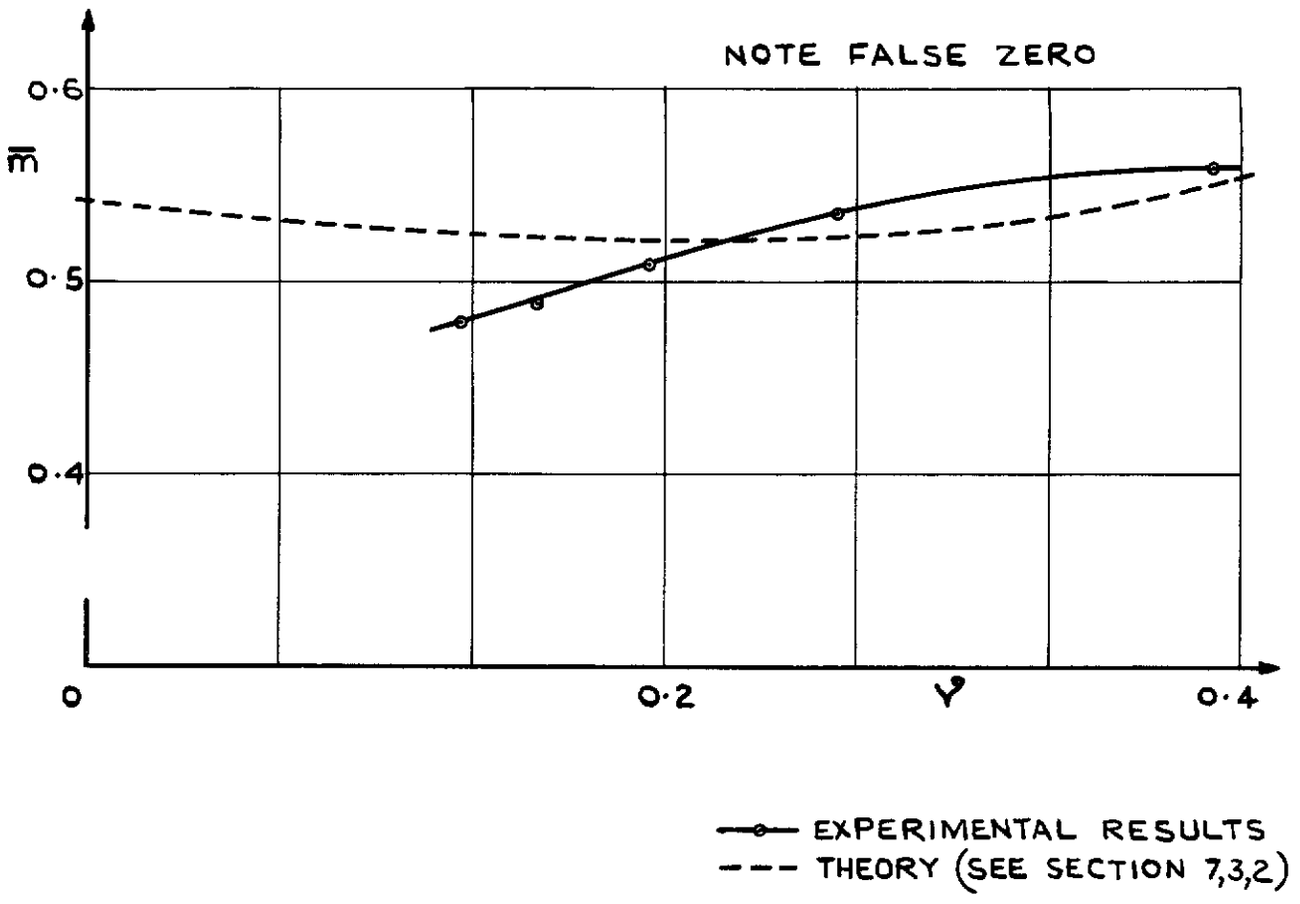

EXPERIMENTAL RESULTS
THEORY (SEE SECTION 7,3,2)

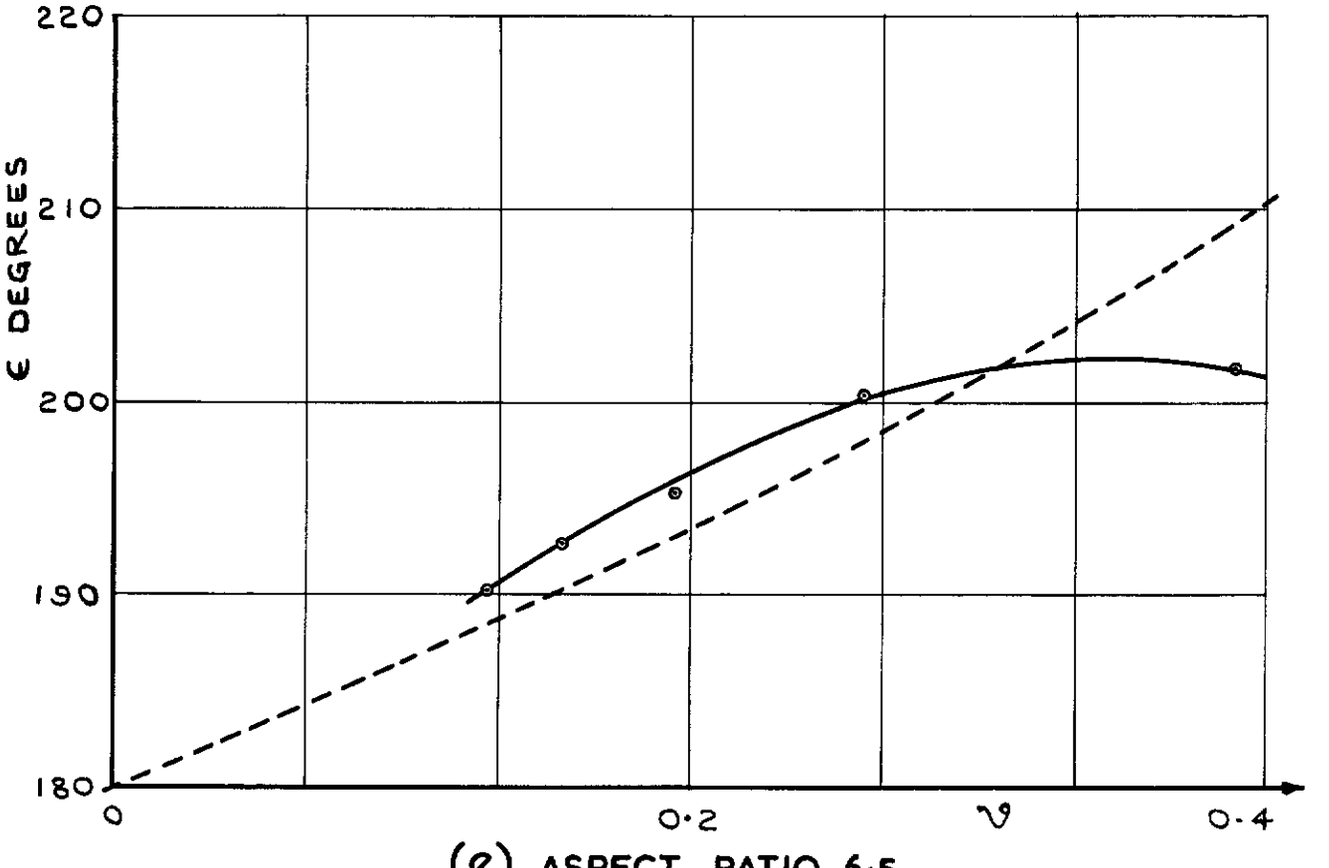

(e) ASPECT RATIO 6·5

FIG. 13 (e) VARIATION OF RESULTANT MOMENT AND PHASE ANGLE WITH FREQUENCY PARAMETER: PITCHING ABOUT LEADING EDGE.

FIG. 13(f)

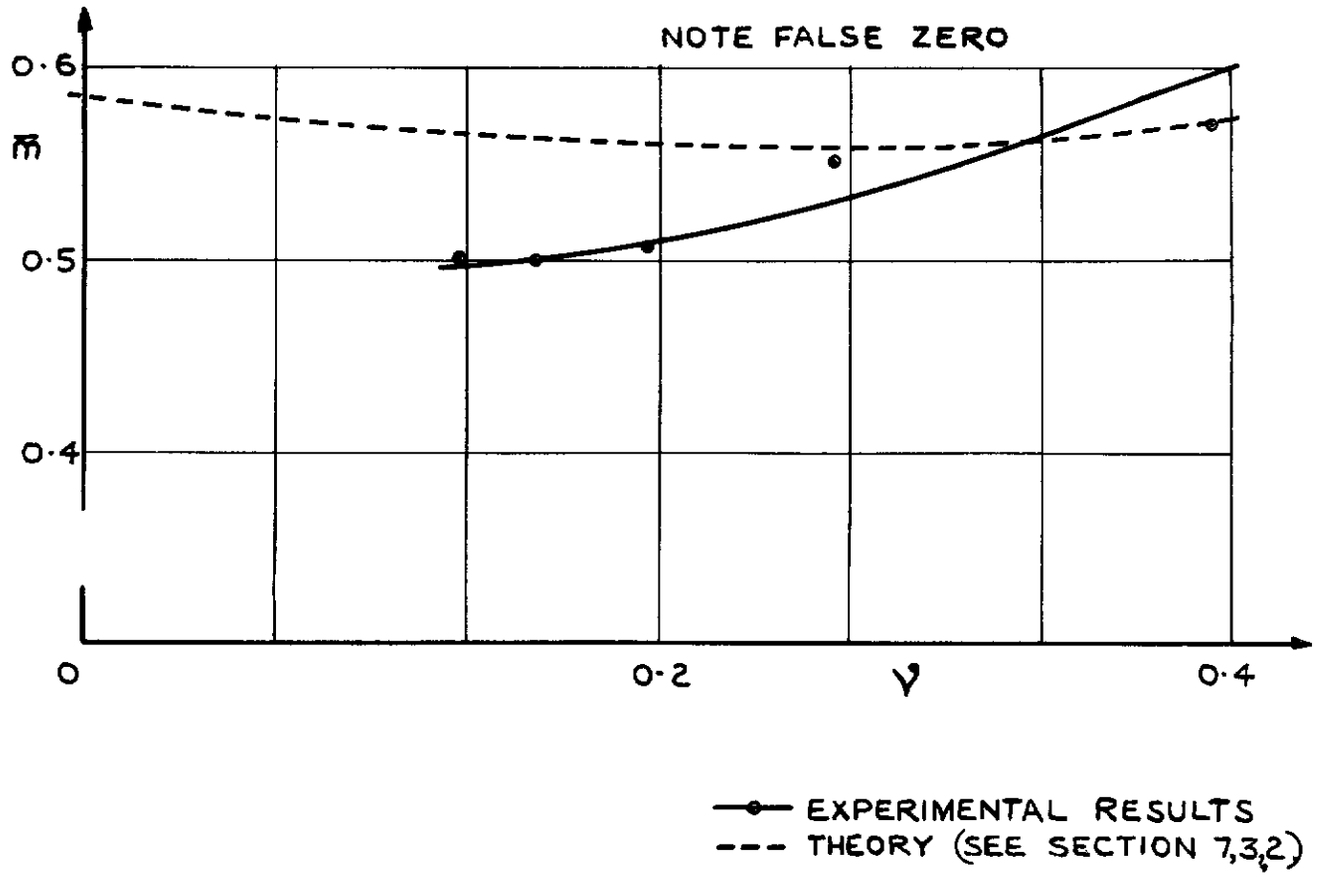

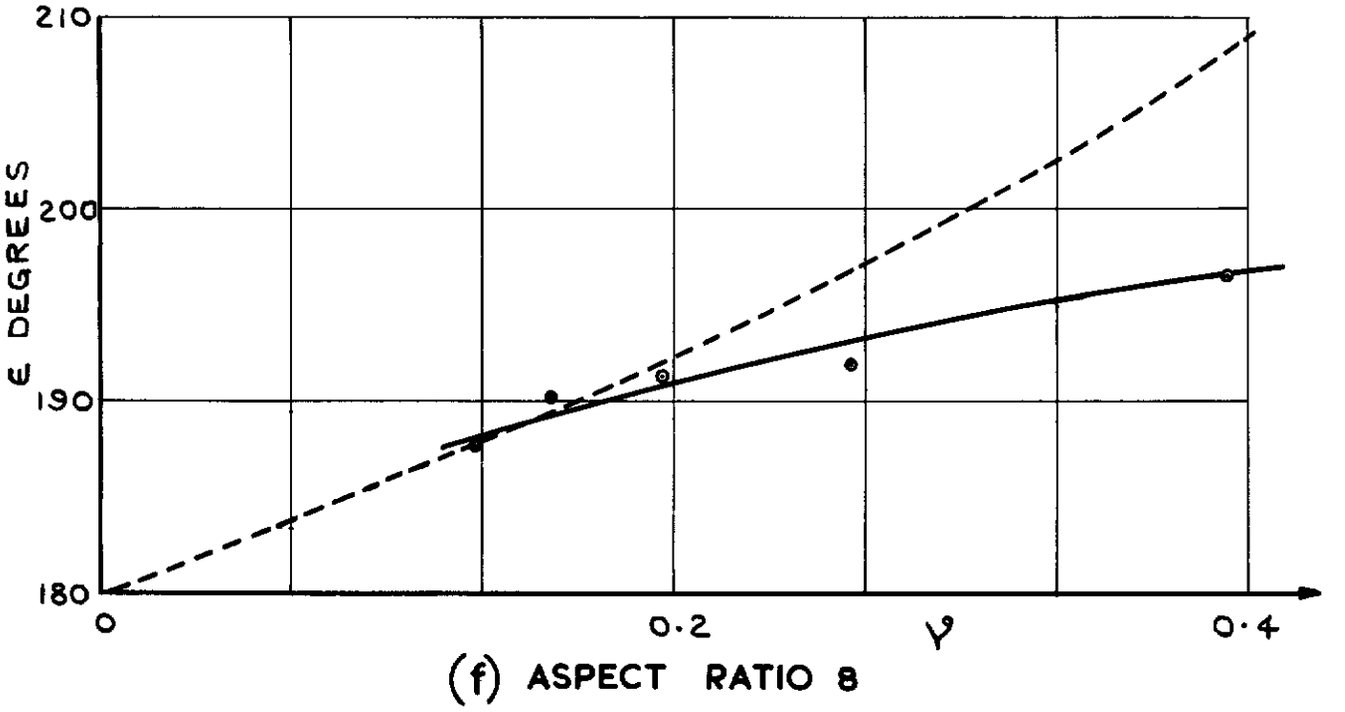

FIG. 13(f) VARIATION OF RESULTANT MOMENT AND PHASE ANGLE WITH FREQUENCY PARAMETER: PITCHING ABOUT LEADING EDGE.

FIG. 13(g)

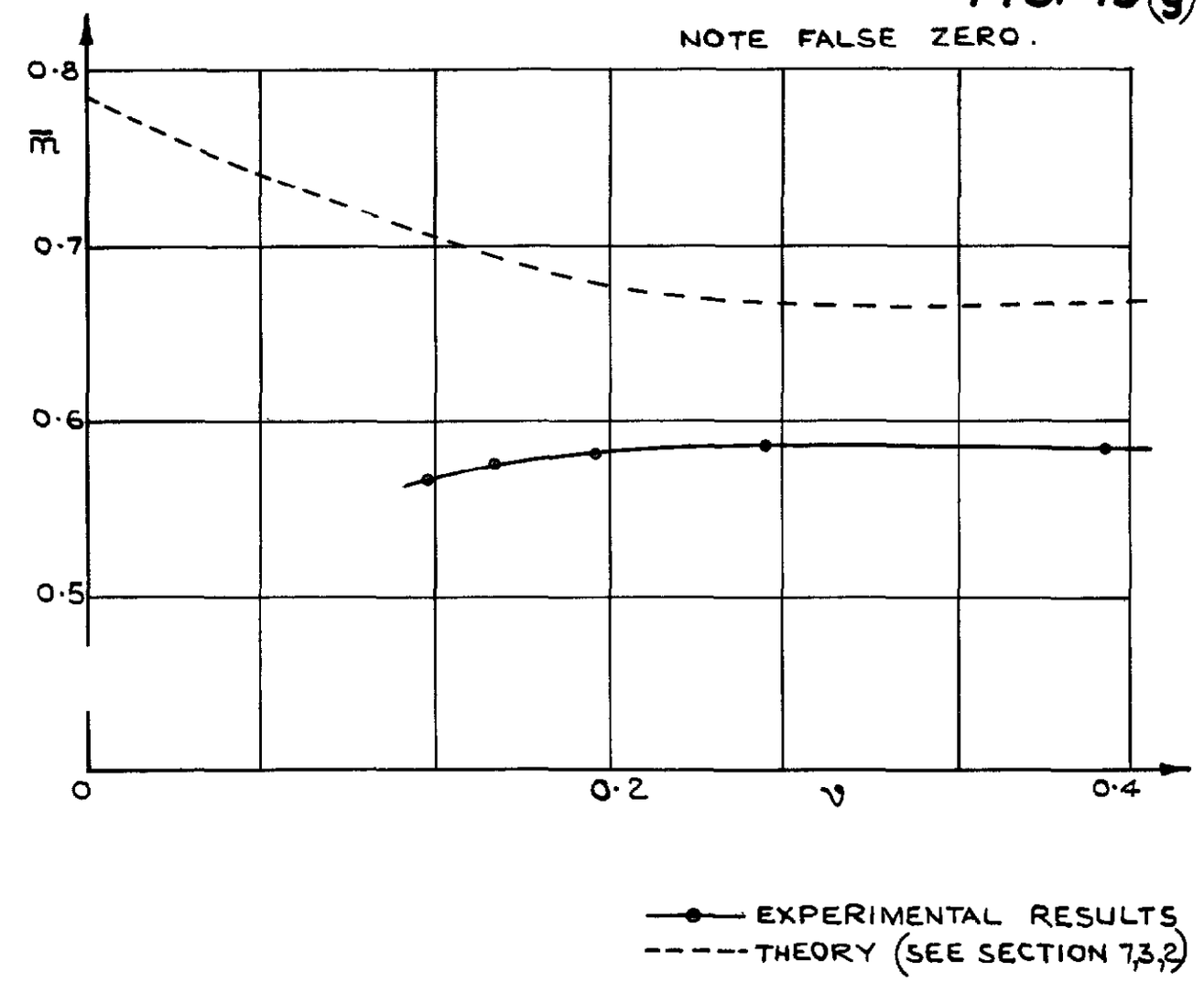

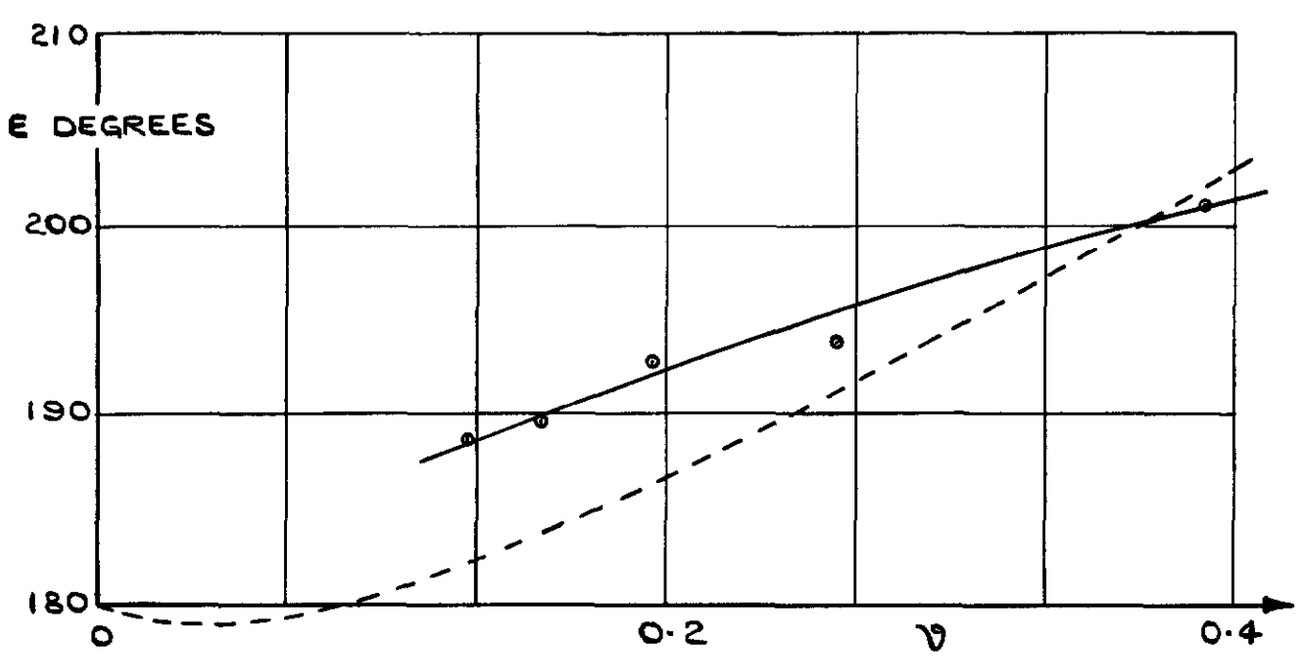

(g) ASPECT RATIO ∞.

FIG. 13(g) VARIATION OF RESULTANT MOMENT AND PHASE ANGLE WITH FREQUENCY PARAMETER: PITCHING ABOUT LEADING EDGE.

FIG. 14(a)

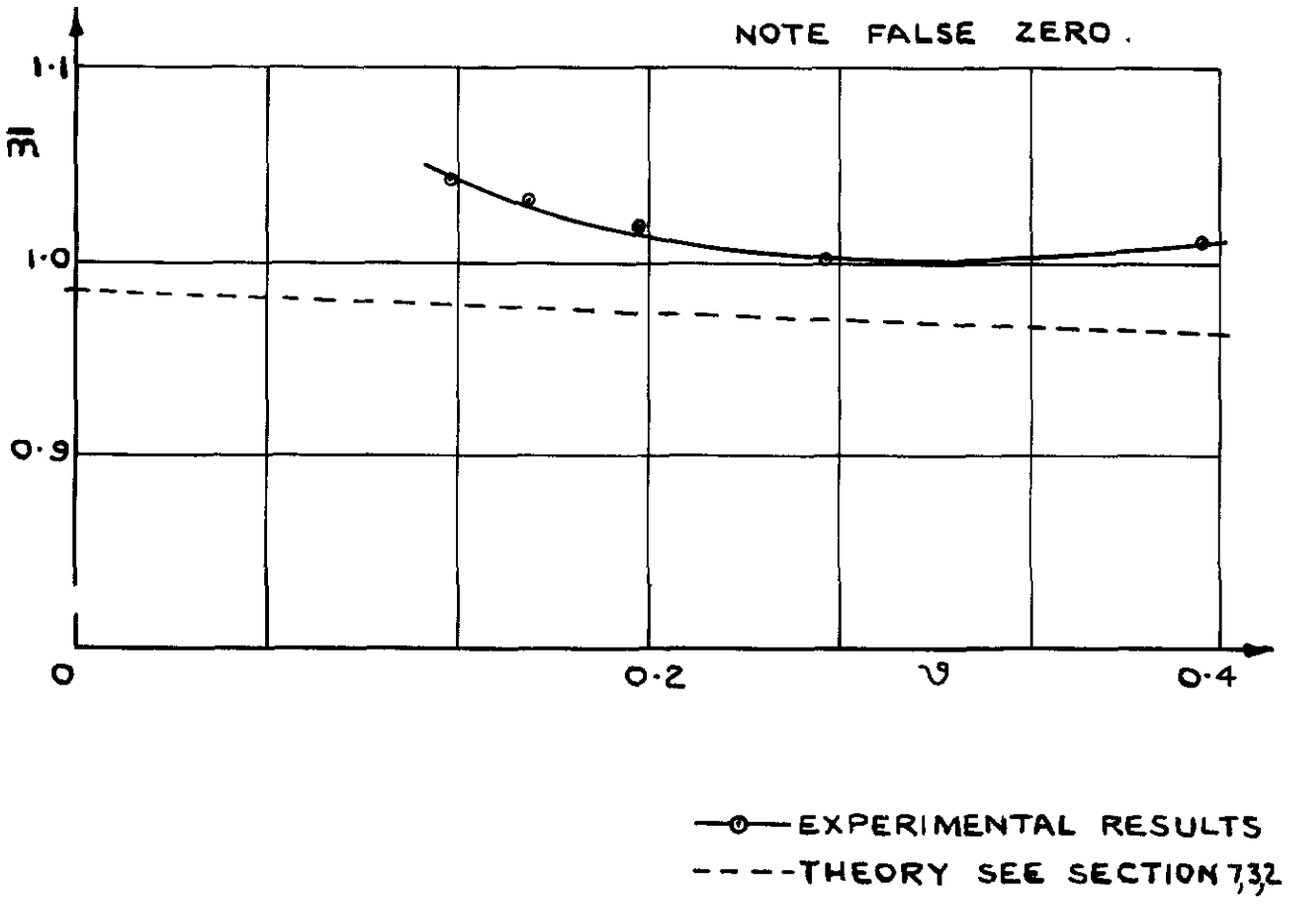

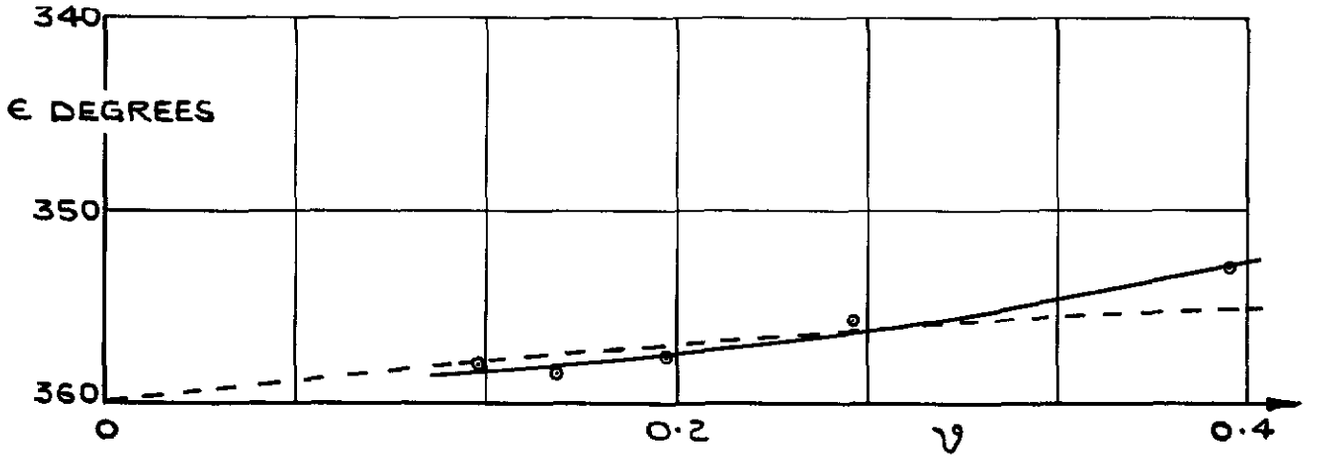

(a) ASPECT RATIO 2.

FIG. 14(a) VARIATION OF RESULTANT MOMENT AND PHASE ANGLE WITH FREQUENCY PARAMETER: PITCHING ABOUT TRAILING EDGE.

FIG. 14. (b)

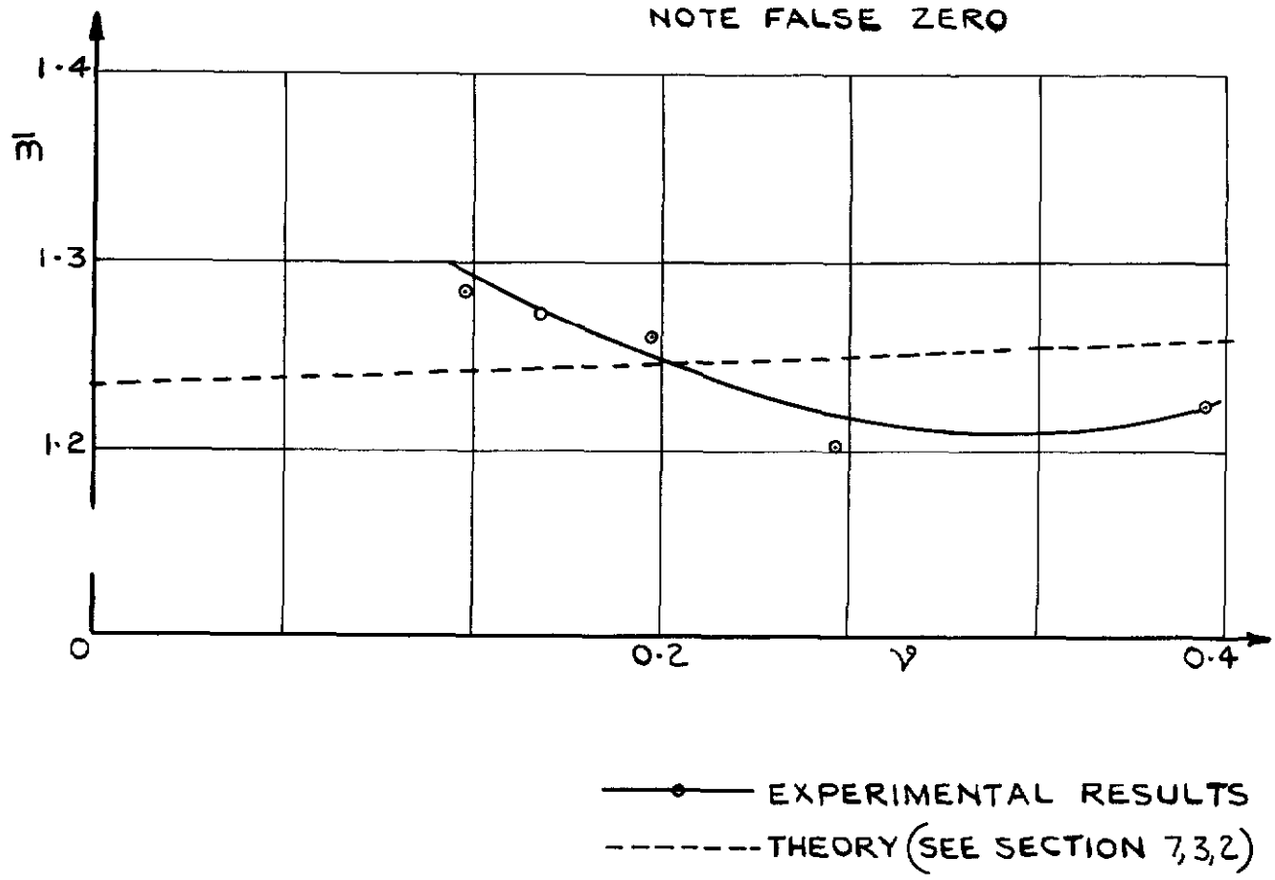

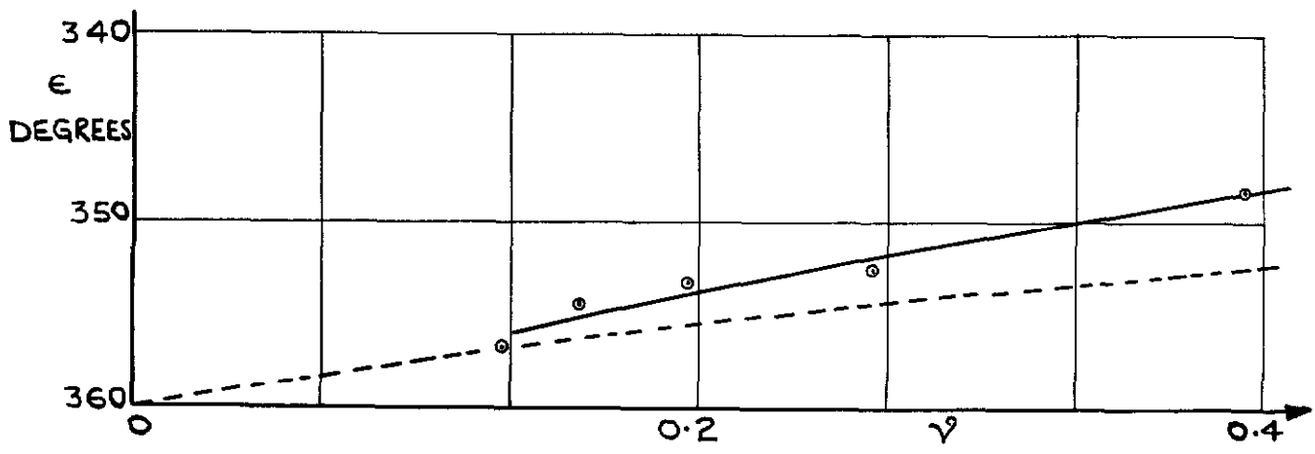

(b) ASPECT RATIO 3·25

FIG. 14. (b) VARIATION OF RESULTANT MOMENT & PHASE ANGLE WITH FREQUENCY PARAMETER: PITCHING ABOUT TRAILING EDGE.

FIG. 14. (c)

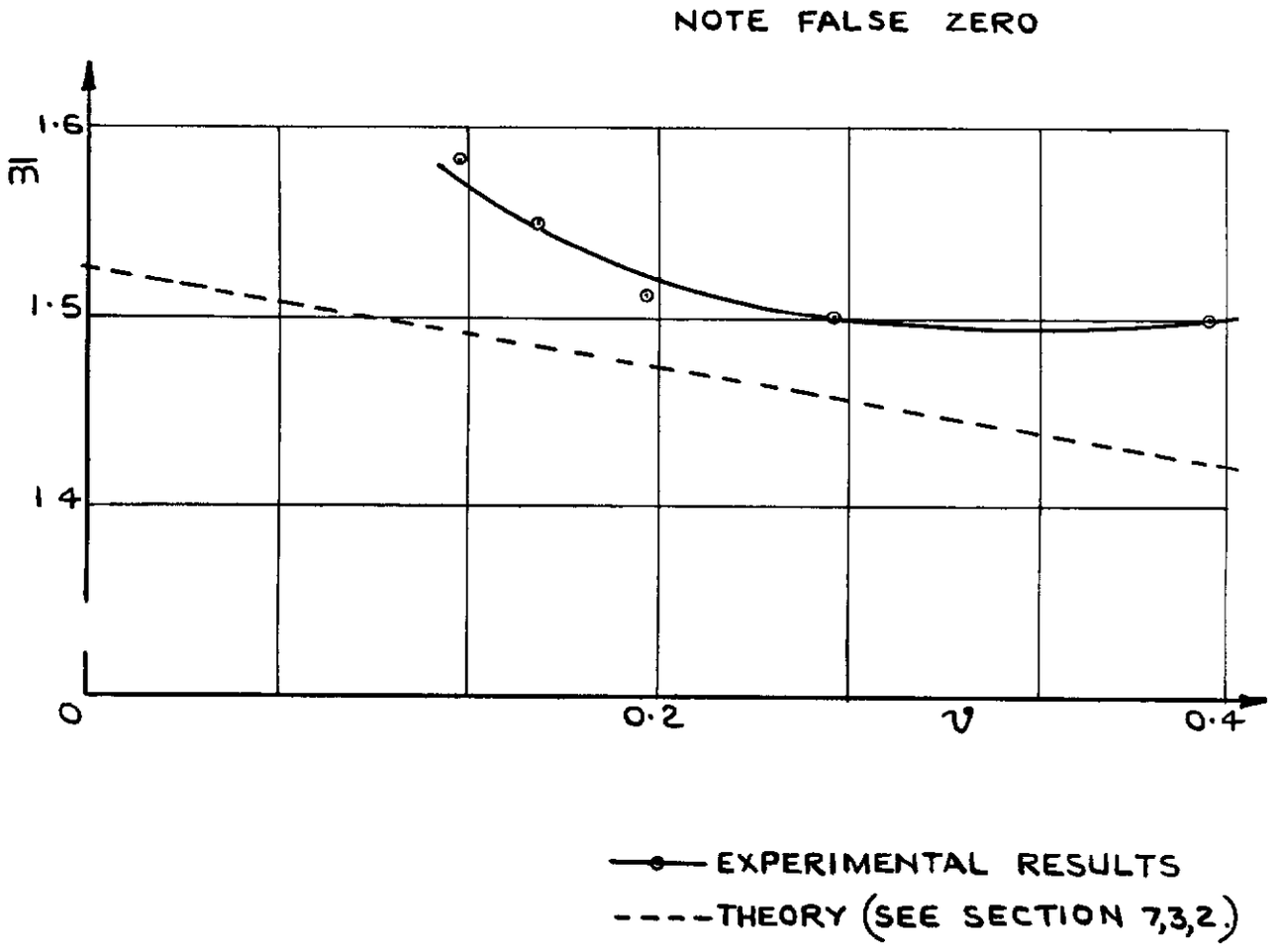

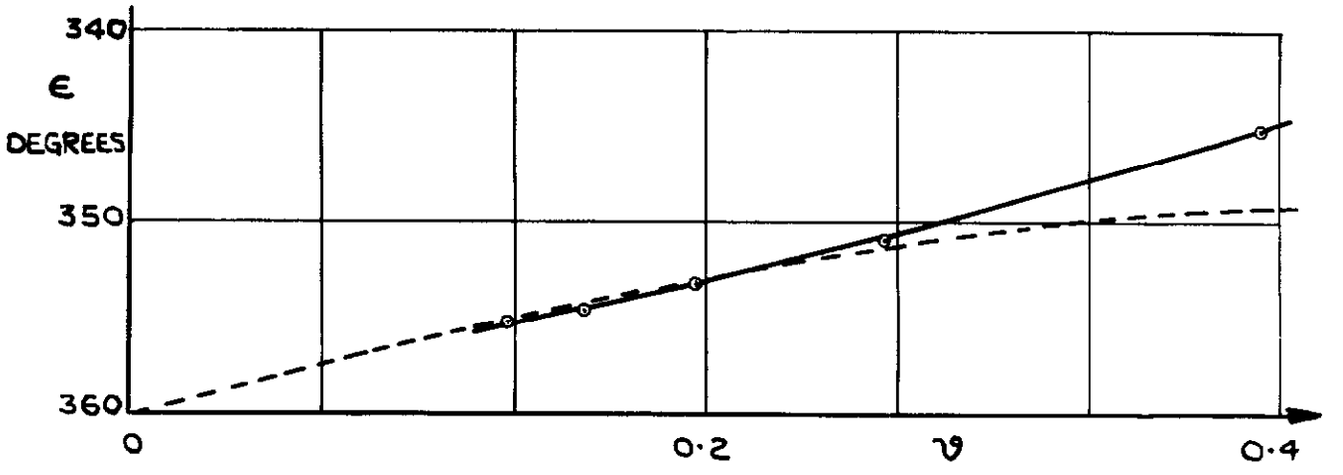

(C) ASPECT RATIO 5

FIG 14 (c) VARIATION OF RESULTANT MOMENT & PHASE ANGLE WITH FREQUENCY PARAMETER: PITCHING ABOUT TRAILING EDGE.

FIG.14.(d)

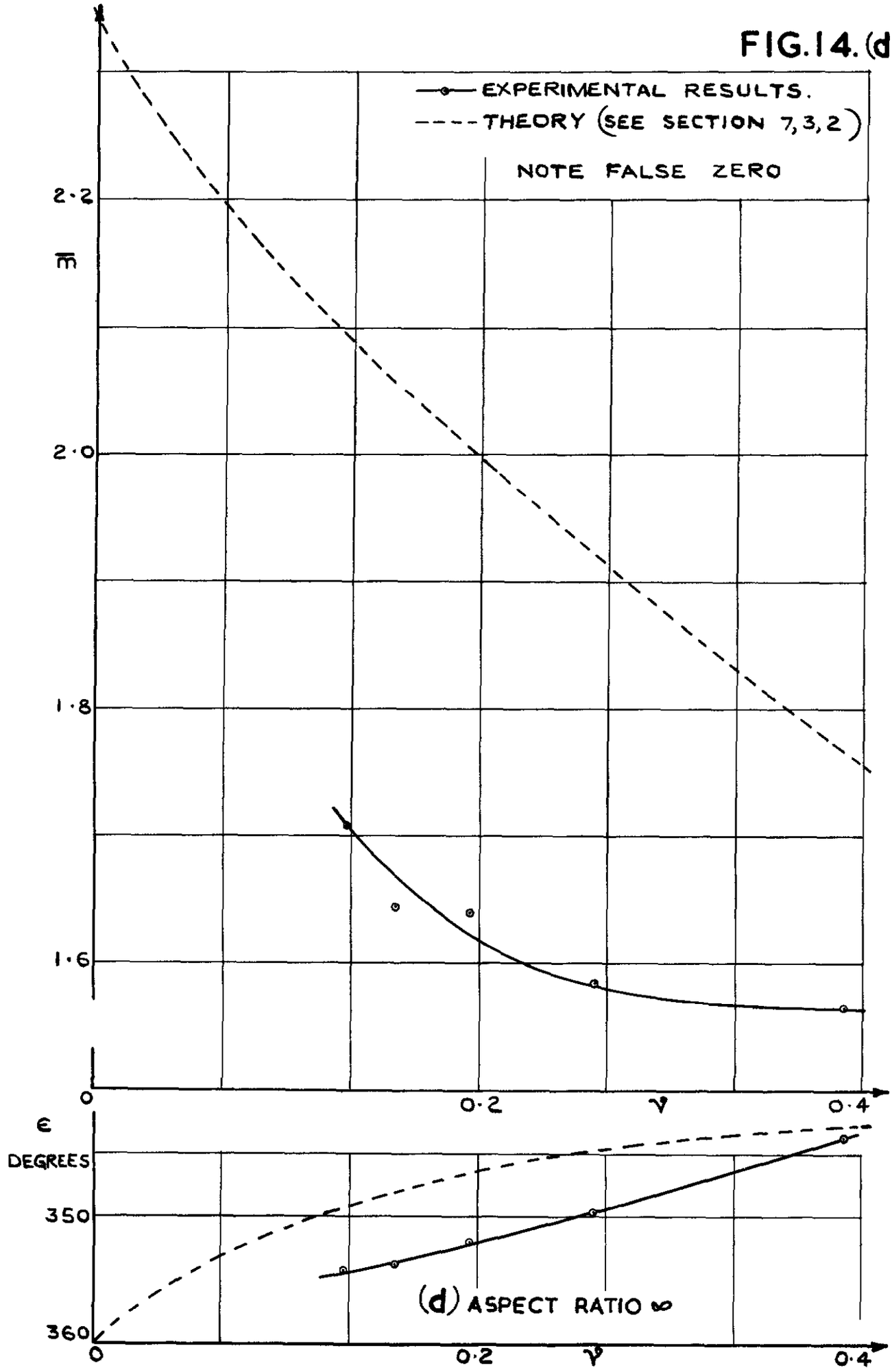

FIG 14(d) VARIATION OF RESULTANT MOMENT & PHASE ANGLE WITH FREQUENCY PARAMETER: PITCHING ABOUT TRAILING EDGE.

FIG. 15.

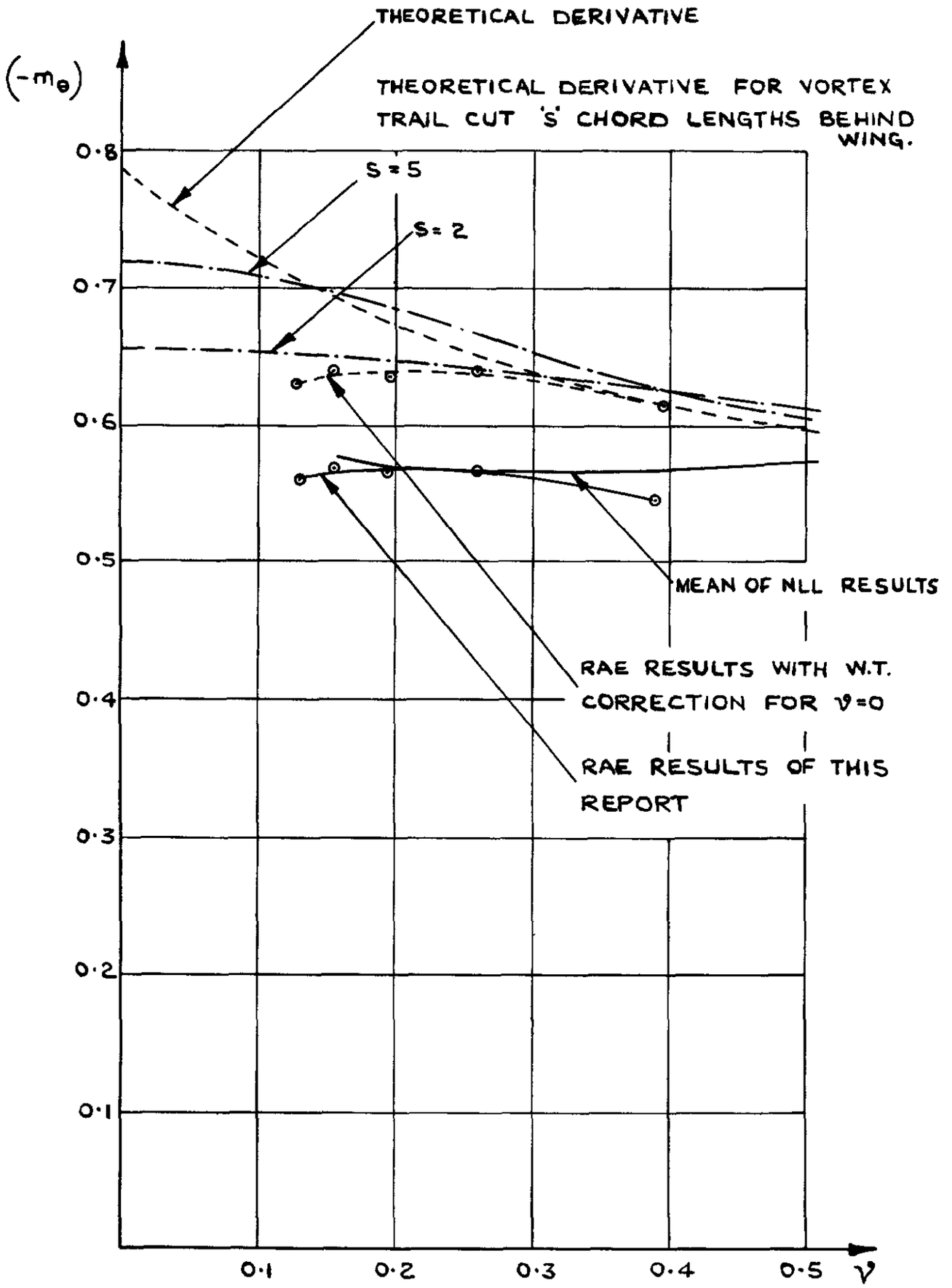

FIG. 15. VARIATION OF $(-m_\theta)$ WITH FREQUENCY PARAMETER FOR WING PITCHING ABOUT ITS LEADING EDGE IN TWO-DIMENSIONAL FLOW.

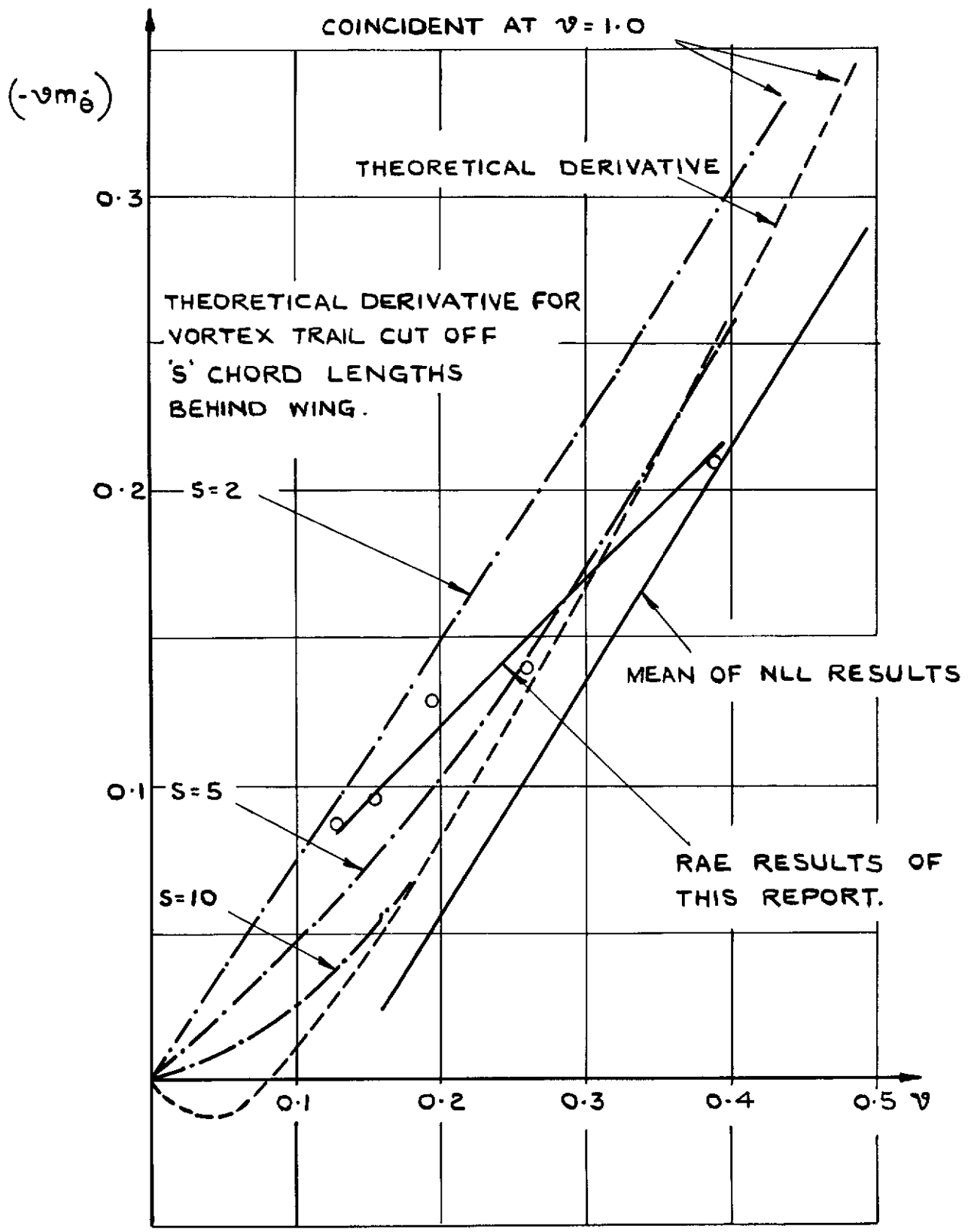

FIG. 16. VARIATION OF $(-\nu m_{\dot{\theta}})$ WITH FREQUENCY PARAMETER FOR WING PITCHING ABOUT ITS LEADING EDGE IN TWO-DIMENSIONAL FLOW.

FIG. 17.

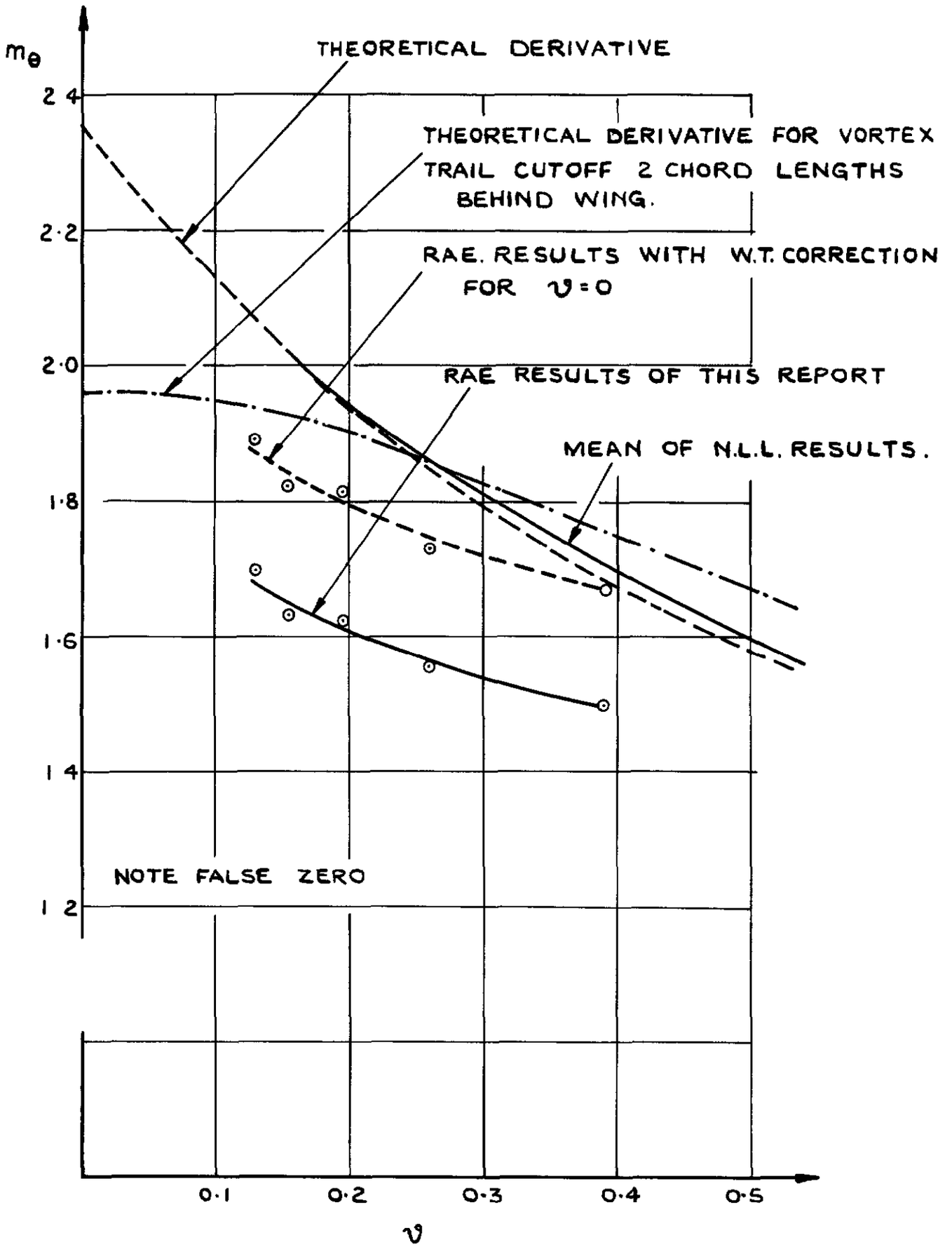

FIG. 17. VARIATION OF m_θ WITH FREQUENCY PARAMETER FOR WING PITCHING ABOUT ITS TRAILING EDGE IN TWO-DIMENSIONAL FLOW.

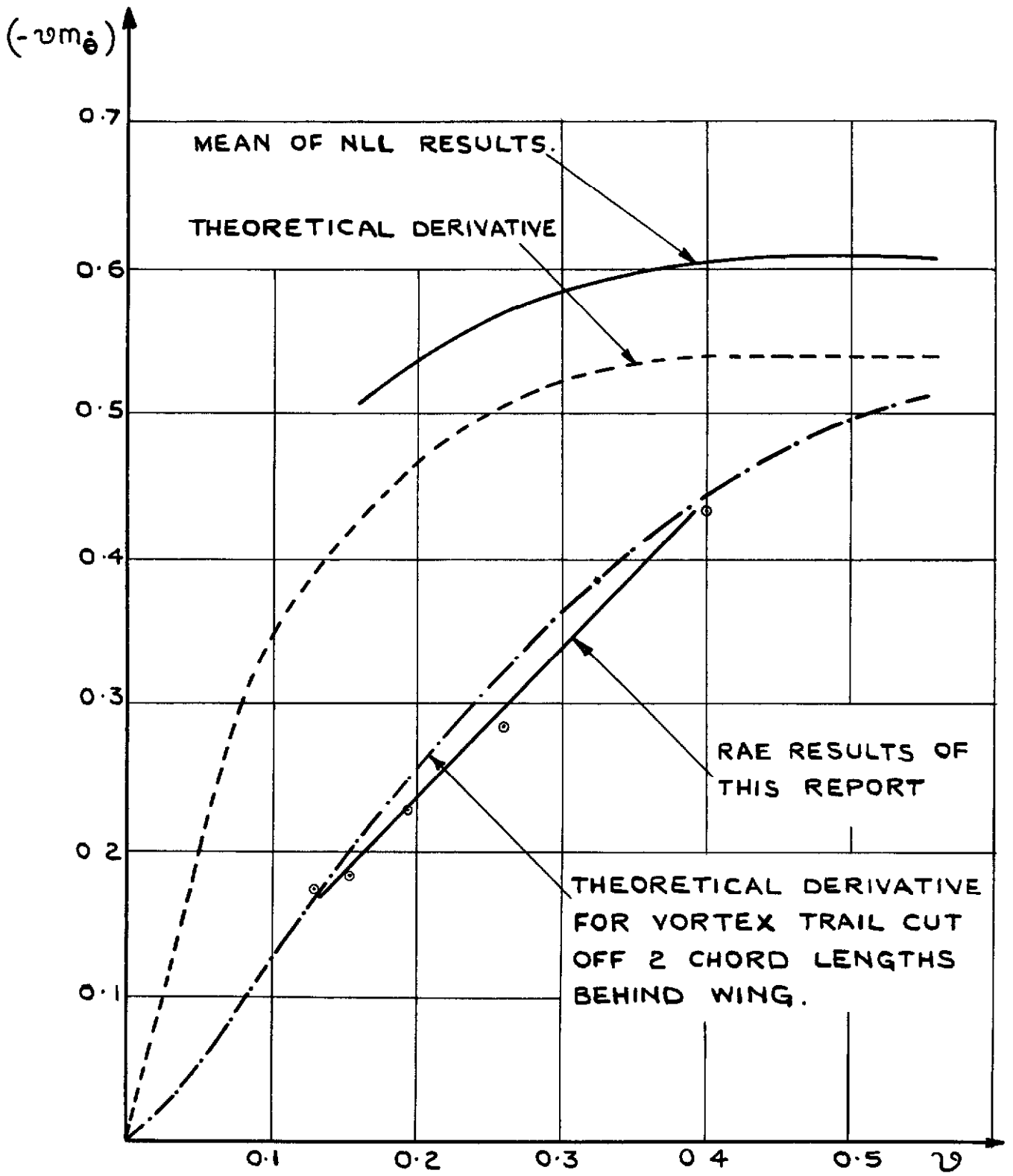

FIG 18. VARIATION OF $(-\upsilon m_{\dot{\theta}})$ WITH FREQUENCY PARAMETER FOR WING PITCHING ABOUT ITS TRAILING EDGE IN TWO-DIMENSIONAL FLOW.

C.P. No. 249
(18,012)
A.R.C. Technical Report

Published by
HER MAJESTY'S STATIONERY OFFICE

To be purchased from
York House, Kingsway, London W C 2
423 Oxford Street, London W 1
P O Box 569, London S.E 1
13A Castle Street, Edinburgh 2
109 St Mary Street, Cardiff
39 King Street, Manchester 2
Tower Lane, Bristol 1
2 Edmund Street, Birmingham 3
80 Chichester Street, Belfast
or through any bookseller

PRINTED IN GREAT BRITAIN

S.O. Code No. 23-9009-49

Wt.2078.K3

C.P. No. 249